Dalton Transactions

ROYAL SOCIETY OF CHEMISTRY

PAPER

View Article Online
View Journal | View Issue

Cite this: *Dalton Trans.*, 2021, **50**, 5557

New organometallic ruthenium(II) complexes with purine analogs – a wide perspective on their biological application†‡

Marzena Fandzloch, *[a] Tomasz Jędrzejewski, [b] Liliana Dobrzańska, [c] Ginés M. Esteban-Parra, [d] Joanna Wiśniewska, [c] Agata Paneth, [e] Piotr Paneth [f] and Jerzy Sitkowski [g,h]

Received 19th November 2020,
Accepted 22nd March 2021

DOI: 10.1039/d0dt03974h

rsc.li/dalton

Three half-sandwich organometallic ruthenium(II) complexes containing purine analogs such as triazolopyrimidines of general formula $[(\eta^6\text{-}p\text{-cym})Ru(L)Cl_2]$, where *p*-cym represents *p*-cymene and L is 5,6,7-trimethyl-1,2,4-triazolo[1,5-*a*]pyrimidine (tmtp for **1**), 5,7-diethyl-1,2,4-triazolo[1,5-*a*]pyrimidine (detp for **2**) and 5-methyl-1,2,4-triazolo[1,5-*a*]pyrimidin-7(4*H*)-one (HmtpO for **3**), have been synthesized and characterized by elemental analysis, infrared, multinuclear magnetic resonance spectroscopic techniques (^1H, ^{13}C, ^{15}N), and single-crystal X-ray diffraction (for **1** and **2**). All these complexes have been thoroughly screened for their *in vitro* cytotoxicity against MCF-7 and HeLa cell lines as well as L929 murine fibroblast cells, indicating $[(\eta^6\text{-}p\text{-cym})Ru(HmtpO)Cl_2]$ (**3**) as the most active representative against the HeLa cell line and simultaneously being 64-fold less toxic to normal L929 murine fibroblast cells than cisplatin. At the same time, **3** has shown antimetastatic activity comparable to NAMI-A against HeLa cells both after 24 and 48 h of treatment in a wound healing assay. In order to better understand the mechanism of anticancer action and differences in the cytotoxic activity of **1–3**, the studies were expanded to determining their lipophilicity, the kinetic stability at pH 6.5–8, the effect on reactive oxygen species (ROS) production in HeLa cells and interactions with significant biomolecules (DNA and albumin) by using molecular docking and circular dichroism (CD) experiments. Furthermore, antiparasitic studies against *L. braziliensis*, *L. infantum* and *T. cruzi* reveal that the newly synthesized complexes **1–3** are very promising candidates which can compete with commercial antiparasitic drugs. Complex **3** in particular, on top of exhibiting a high antiparasitic effect (IC_{50} < 1 μM against two strains), reaches a selectivity index >1000.

Introduction

Due to acquired or intrinsic resistance and severe side effects during cisplatin-based therapy and other platinum-based drugs, it has become a challenge to search for selective and safer drugs with larger therapeutic windows.[1–3] Ruthenium complexes appear an interesting alternative, with properties that allow these to compete with platinum complexes, including *e.g.* the ability to mimic iron by binding to biological molecules, reduced general toxicity and stronger affinity to cancer tissues than normal tissues, a variety of oxidation states of ruthenium ions, tunable redox properties, a wide range of coordination numbers and structural diversity modulated by coordinating ligands.[4,5] The endless interest in agents based

[a]*Institute of Low Temperature and Structure Research, Polish Academy of Sciences, Okólna 2, 50-422 Wrocław, Poland. E-mail: m.fandzloch@intibs.pl*
[b]*Department of Immunology, Faculty of Biological and Veterinary Sciences, Nicolaus Copernicus University in Toruń, Lwowska 1, 87-100 Toruń, Poland*
[c]*Faculty of Chemistry, Nicolaus Copernicus University in Toruń, Gagarina 7, 87-100 Toruń, Poland*
[d]*Department of Inorganic Chemistry, University of Granada, Avda. Severo Ochoa s/n, 18071 Granada, Spain*
[e]*Department of Organic Chemistry, Faculty of Pharmacy, Medical University of Lublin, Chodźki 4a, 20-093 Lublin, Poland*
[f]*Institute of Applied Radiation Chemistry, Faculty of Chemistry, Lodz University of Technology, Żeromskiego 116, 90-924 Lodz, Poland*
[g]*National Institutes of Medicines, Chełmska 30/34, 00-725 Warszawa, Poland*
[h]*Institute of Organic Chemistry, Polish Academy of Sciences, Kasprzaka 44/52, 01-224 Warszawa, Poland*

†In memoriam of Professor Juan Manuel Salas Peregrín and his contributions to the research on triazolopyrimidines.

‡Electronic supplementary information (ESI) available: Data of lipophilicity details, the fit for the dose–response curves for data obtained during the MTT and LDH test, molecular docking-validation; quantum mechanical calculations; ^1H, ^{13}C, ^{15}N NMR spectra for **1–3**; kinetic and fit trace for **1**, ESI-MS spectra for **1**; electronic spectra for **2** and **3**; overlay of molecular cores of **1** and **2**, molecular packing data, CD spectra for **1–3**. CCDC 2041839 and 2041840. For ESI and crystallographic data in CIF or other electronic format see DOI: 10.1039/d0dt03974h

on ruthenium has been triggered by the results of three ruthenium(III) complexes which completed phase I and II clinical trials[6–8] namely NAMI-A ([ImH][*trans*-Ru(dmso)(Im)Cl_4], where Im – imidazole), which acts on solid metastatic tumors,[9] KP1019 ([IndH][*trans*-Ru(Ind)$_2Cl_4$], Ind – indazole), which is effective against resistant tumors[10] and NKP-1339 Na[*trans*-$RuCl_4(Ind)_2$], which shows promising results against non-small cell lung cancer, colorectal carcinoma, and most distinctively in gastrointestinal neuroendocrine tumors.[11] Clarke has proposed that the activity of Ru(III) complexes, which are usually relatively inert towards ligand substitution, is dependent on *in vivo* reduction to more labile Ru(II) complexes.[12–17] It should be remembered, however, that the kinetic lability of metal ions is highly dependent on the types of bound ligands.[14]

Importantly, the presence of arene can stabilize the whole structure as well as the ruthenium oxidation state, and increases the hydrophobicity of the complex, facilitating passage across cell membranes.[16,17]

Interest in organometallic Ru(II) complexes that adopt the piano-stool geometry was initiated by work on [Ru(η^6-C_6H_6)(metronidazole)Cl_2] published in 1992 by Dale *et al.*[18] Notably, due to research developed by Sadler[19] and Dyson,[20] the chemistry of ruthenium(II) organometallic complexes has become very important. Among complexes with three-legged piano-stool geometry, a lot of studies have been devoted to the family of RAPTA complexes of general formula [Ru(η^6-arene)Cl_2(PTA)] (PTA = 1,3,5-triaza-7-phosphaadamantane).[21] These kinds of Ru(II) complexes generally exhibit low *in vitro* cytotoxicity,[22] but relevant antimetastatic,[23,24] and antiangiogenic[25] properties *in vivo*. The lead compound RAPTA-C, [Ru(η^6-*p*-cym)Cl_2(PTA)], has been shown to reduce the growth of primary tumors in preclinical models for ovarian and colorectal carcinomas *via* an antiangiogenic mechanism.[26]

Despite the promising pharmacological properties of ruthenium(II)-arene compounds, further enhancing their efficacy and selectivity is important. To achieve this, the structure was modified by introducing lipophilic chains on the ruthenium (II)-arene complexes, *via* modification of PTA,[27] imidazole,[28] or isonicotinic ester[29,30] ligands, leading to increased antiproliferative activity, presumably due to greater than before cellular uptake, but not necessarily to improved cancer cell selectivity.

In our previous studies, we successfully demonstrated the synergistic effects of purine analogs such as triazolopyrimidines and ruthenium of different oxidation states on anticancer properties.[31,32] These N-donor ligands, specifically 1,2,4-triazolo[1,5-*a*]pyrimidine derivatives, display great versatility in their interactions with metal ions. Moreover, compounds containing this core exhibit biological activity in a variety of therapeutic domains (anticancer, antiparasitic, antibacterial, antifungal, antiviral, *etc.*), providing many potential applications.[33]

Researchers from the University of Granada have taken this into account and have used the potential of complexes of various metals with triazolopyrimidines to develop new antiparasitic drugs.[34–38] This is a significant challenge as Leishmaniasis and Chagas disease are responsible for substantial global morbidity, mortality, and economic adversity in tropical and subtropical regions.[39] Unfortunately, the current drugs used to treat these diseases are associated with significant limitations in their use, such as toxicity problems, limited efficacy and resistance of certain parasite strains.[40,41] Literature data indicate that ruthenium complexes may be promising in this respect,[42] but the limited amount of data, especially for ruthenium complexes with triazolopyrimidines, indicates the need to explore this approach.

Herein, we present the synthesis and structural characterization of three new Ru(II) complexes of general formula [(η^6-*p*-cym)Ru(L)Cl_2], where L = 5,6,7-trimethyl-1,2,4-triazolo[1,5-*a*]pyrimidine (tmtp for **1**), 5,7-diethyl-1,2,4-triazolo[1,5-*a*]pyrimidine (detp for **2**) and 5-methyl-1,2,4-triazolo[1,5-*a*]pyrimidin-7(4*H*)-one (HmtpO for **3**). We present a wide range of profiling in support of their future biological applications through (i) *in vitro* cytotoxicity studies against cancer as well as normal cell lines, based on MTT and LDH assays, wound healing assay, lipophilicity, ability to ROS generation; (ii) identification of the interactions with important primary target molecules of many anticancer agents, such as albumin and DNA, by means of molecular docking and circular dichroism; (iii) *in vitro* antiparasitic studies.

Experimental

Materials and physical measurements

7-Hydroxy-5-methyl-1,2,4-triazolo[1,5-*a*]pyrimidine (HmtpO) (98%), 3-amino-1,2,4-triazole (95%), 3,5-heptanedione (98%), α-terpinene (85%), 1-octanol (≥99%), CT-DNA, bovine serum albumin (98%) and all other analytical-grade chemicals and solvents were purchased from Sigma-Aldrich. 3-Methyl-2,4-pentanedione (96%) was purchased from TCI Co. Ruthenium(III) chloride hydrate was purchased from Apeiron Synthesis S.A. Sodium chloride (99.5%) and hydrochloric acid (35–38%) was purchased from Avantor Performance Materials Poland S.A. Phosphate buffered solution was prepared from sodium phosphate monobasic monohydrate (≥99%) and sodium phosphate dibasic heptahydrate (98.0–102.0%) or sodium phosphate dibasic (≥99%) purchased from Sigma-Aldrich. The phosphate buffer (10 mM, pH = 7.4) was prepared from $NaH_2PO_4 \cdot H_2O$ and Na_2HPO_4 dissolved in ultrapure water (18.2 MΩ) in quantities according to buffer calculator.[43]

The syntheses of the ligands detp[44] and tmtp[45] were carried out using an established condensation procedure[46] involving the reaction of 3-amino-1,2,4-triazole with the appropriate dione. Dimeric ruthenium(II)-arene precursor, [{(η^6-*p*-cym)Ru(μ-Cl)}$_2Cl_2$], was prepared according to the method reported by Bennett through the reaction of ruthenium(III) chloride with α-terpinene.[47] NAMI-A used as a reference was prepared according to the previously reported procedure.[48]

The contents of C, H, and N were determined by elemental semimicroanalysis; IR spectra were recorded with a Bruker Vertex 70v FT-IR on an ATR unit (Diamond) spectrometer (4000–400 cm^{-1}) and with Bruker 66/s FT-IR spectrometer

(600–50 cm^{-1} in Nujol). NMR spectra were recorded at 298 K in $CDCl_3$ solutions with a Varian VNMRS-500 spectrometer operated at 499.8, 125.7 and 50.6 MHz for ^1H, ^{13}C, and ^{15}N, respectively. The reference standards were TMS for ^1H and ^{13}C, and CH_3NO_2 for ^{15}N. Standard Varian pulse sequences were used except the ^1H–{^{15}N} HMBC correlation. Gradient-enhanced IMPACT-HMBC[49] ^1H–{^{15}N} correlation spectra were optimized for a coupling constant of 6 Hz under the following experimental conditions: an acquisition time of 0.2 s, spectral windows of 6000 (F2) and 10 000 (F1) Hz, 1 K complex data points, 256 time increments, 30 ms WURST-2 mixing sequence centred within the 60 ms preparation interval (ASAP2) and a 150 Ernst angle as the excitation pulse.[50] UV–Vis spectra were obtained with a Biobase double beam BK-D590 UV–Vis spectrophotometer, using a quartz cuvette with a path length of 1.0 cm. Mass spectrometry analyses were performed using Synapt G2-S HDMS mass spectrometer (Waters) equipped with the electrospray ion source and quadrupole-time-of-flight mass analyzer. The resolving power of the TOF analyzer was 20 000 FWHM. Acetonitrile was used as a mobile phase with a flow rate of 100 μl min^{-1}. The measurement was performed both in the positive and negative ion modes. The measurement in the positive mode was performed with a capillary voltage set to 3.5 kV. The desolvation gas flow was 750 L h^{-1} and temperature 350 °C. The sampling cone voltage and source offset were set to 100 V and the source temperature was 120 °C. The measurement in the negative ion mode was performed with a capillary voltage set to 3.0 kV. The desolvation gas flow was 550 L h^{-1} and temperature 350 °C. The sampling cone voltage and source offset were set to 50 V, and the source temperature was 120 °C. The Leucine-Enkephaline solution was used as the Lock-Spray reference material. The circular dichroism (CD) spectra were performed on Jasco J-715 spectropolarimeter.

Preparation of new ruthenium complexes

Starting compounds, $RuCl_3{\cdot}xH_2O$ and triazolopyrimidine derivatives (tmtp, detp and HmtpO) were used as substrates for the syntheses of new Ru(II) complexes of general formula $[(\eta^6\text{-}p\text{-cym})Ru(L)Cl_2]$, where L = tmtp for **1**, detp for **2** and HmtpO for **3** (Scheme 1, details below).

$[(\eta^6\text{-}p\text{-cym})Ru(tmtp)Cl_2]$ (1). To $[(\eta^6\text{-}p\text{-cym})RuCl_2]_2$ (0.312 g, 0.49 mmol) solved in isopropanol (40 mL) at 60–70 °C tmtp solution (0.160 g, 0.98 mmol in 10 mL of isopropanol) was added and the mixture was stirred for 24 h at 60 °C. The brownish red powder formed was filtered off, washed with diethyl ether (10 mL) and dried in air (yield: 0.417 g, 90%). Monocrystals suitable for X-ray crystallography were obtained by slow evaporation of the filtrate at r.t. Found: C, 46.43; H, 5.28; N, 11.73. $C_{18}H_{24}N_4Cl_2Ru$ requires C, 46.16; H, 5.16; N, 11.96%. IR (selected bands, ν_{max}/cm^{-1}): 1615m (CN), 1536vs (CC), 1527vs (CC), 486m (RuN), 459m (RuN), 422w (RuN), 321w (RuCl). ^1H NMR (499.8 MHz, $CDCl_3$) δ ppm 8.58 (1H, s, H2), 5.88 (2H, m 2 CH (*p*-cym)), 5.66 (2H, m, 2 CH (*p*-cym), 2.98/1.16 (1H, sep, CH/6H, d, 2 CH_3 (*p*-cym)), 2.744 (3H, s, CH_3(5)), 2.737 (3H, s, CH_3(7)), 2.36 (3H, s, CH_3(6)), 2.21 (3H, s, CH_3 (*p*-cym). ^{13}C NMR (125.7 MHz, $CDCl_3$) δ ppm 166.2/25.0 (C5/CH_3(5)), 155.2 (C2), 152.2 (C3a), 145.6/14.1 (C7/CH_3(7)), 118.8/14.1 (C6/CH_3(6)), 102.7/30.6/22.1 (C/CH/2 CH_3(*p*-cym)), 97.4/18.7 (C/CH_3), 81.7 (2 CH), 81.0 (2 CH). ^{15}N NMR (50.6 MHz, $CDCl_3$) δ ppm −111.8 (N1), −117.8 (N4), −154.3 (N8), −218.8 (N3).

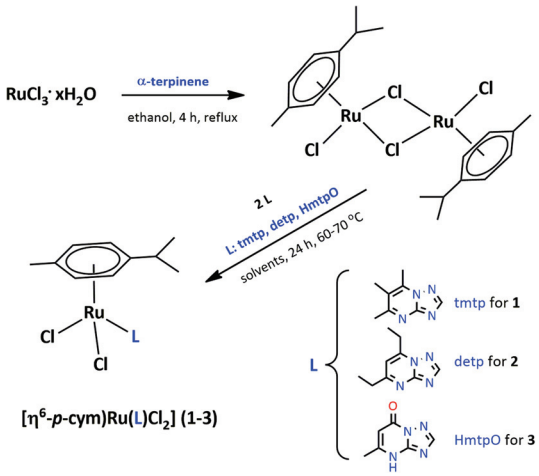

Scheme 1 Synthetic methodology for complexes **1–3** and structural formula of used triazolopyrimidines.

$[(\eta^6\text{-}p\text{-cym})Ru(detp)Cl_2]$ (2). To $[(\eta^6\text{-}p\text{-cym})RuCl_2]_2$ (0.300 g, 0.49 mmol) solved in isopropanol (40 mL) at 60–70 °C detp solution (0.173 g, 0.98 mmol in 10 mL of isopropanol) was added and the mixture was stirred for 24 h at 60 °C. The brownish red powder formed was filtered off, washed with diethyl ether (10 mL) and dried in air (yield: 0.390 g, 83%). Monocrystals suitable for X-ray crystallography were obtained by slow evaporation of the filtrate at r.t. Found: C, 47.00; H, 5.48; N, 11.94. $C_{19}H_{26}N_4Cl_2Ru$ requires C, 47.30; H, 5.43; N, 11.61%. IR (selected bands, ν_{max}/cm^{-1}): 1619s (CN), 1551vs (CC), 490w (RuN), 459w (RuN), 448w (RuN), 320vw (RuCl). ^1H NMR (499.8 MHz, $CDCl_3$) δ ppm 8.62 (1H, s, H2), 6.97 (1H, s, H6), 5.96 (2H, m, 2 CH (*p*-cym)), 5.68 (2H, m, 2 CH (*p*-cym), 3.13 (2H, q, CH2(7)), 3.08 (2H, q, CH_2(5)), 3.02/1.17 (1H, sep, CH/6H, d, 2 CH_3 (*p*-cym)), 2.21 (3H, s, CH_3 (*p*-cym), 1.47 (3H, t, CH_3(5)), 1.38 (3H, t, CH_3(7). ^{13}C NMR (125.7 MHz, $CDCl_3$) δ ppm 171.3/31.8/12.4 (C5/CH_2(5)/CH_3(5)), 156.2 (C2), 154.3 (C3a), 153.5/23.7/10.4 (C7/CH_2(7)/CH_3(7)), 109.3 (C6), 102.8/30.5/22.1 (C/CH/2 CH_3 (*p*-cym)), 97.6/18.7 (C/CH_3), 81.7 (2 CH), 80.8 (2 CH). ^{15}N NMR (50.6 MHz, $CDCl_3$) δ ppm −113.0 (N1), −119.6 (N4), −156.5 (N8), −217.1 (N3).

$[(\eta^6\text{-}p\text{-cym})Ru(HmtpO)Cl_2]$ (3). To $[(\eta^6\text{-}p\text{-cym})RuCl_2]_2$ (0.292 g, 0.47 mmol) solved in isopropanol (40 mL) at 70 °C HmtpO solution (0.143 g, 0.95 mmol in 15 mL of 1 M HCl) was added and the mixture was stirred for 24 h at 70 °C. To avoid ligand precipitation it was important to maintain a temperature no lower than 70 °C during 24 h. The orange powder formed was filtered off, washed with ethanol (10 mL) and dried in air (yield: 0.137 g, 64%). Found: C, 41.85; H, 4.74; N, 11.99. $C_{16}H_{20}N_4OCl_2Ru$ requires C, 42.11; H, 4.42; N,

12.28%. IR (selected bands, ν_{max}/cm^{-1}): 1730vs (CO), 1640s (CN), 1580vs (CC), 476w (RuN), 456vw (RuN), 446vw (RuN), 316vw (RuCl). ^{1}H NMR (499.8 MHz, $CDCl_3$) δ ppm 11.62 (1H, s, NH(4)), 8.31 (1H, s, H2), 5.80 (1H, s, H6), 5.59 (2H, m, 2 CH (*p*-cym)), 5.43 (2H, m, 2 CH (*p*-cym), 3.05/1.31 (1H, sep, CH/6H, d, 2 CH_3 (*p*-cym)), 2.33 (3H, s, CH_3(5)), 2.28 (3H, s, CH_3 (*p*-cym). ^{13}C NMR (125.7 MHz, $CDCl_3$) δ ppm 154.6 (C7), 153.0 (C2), 151.0 (C3a), 149.9/19.8 (C5/CH_3(5)), 104.2/30.8/22.2 (C/CH/2 CH_3 (*p*-cym)), 100.5 (C6), 98.5/18.8 (C/CH_3), 82.3 (2 CH), 81.6 (2 CH). ^{15}N NMR (50.6 MHz, $CDCl_3$) δ ppm −110.0 (N1), −155.4 (N8), −233.6 (N3), −251.8 (N4).

X-ray structure determination

Single-crystal X-ray diffraction data for **1** and **2** were collected on an Oxford Diffraction Xcalibur diffractometer equipped with a Sapphire 2 CCD area detector with graphite monochromated MoKα radiation (λ = 0.7107 Å). The CrysAlisPro software system was used for data collections, cell refinements, and data reductions.[51] Empirical absorption corrections were applied. The structures were solved using the direct method with SHELXS-2018/3 [52] and refined by full-matrix least-squares methods based on F^2 with SHELXL-2018/3.[53] All non-hydrogen atoms were refined anisotropically. Hydrogen atoms were placed in calculated positions with displacement factors fixed at 1.2 times U_{eq} of the parent C atoms and 1.5 times U_{eq} for methyl groups with C–H = 0.93 Å (aromatic), 0.96 Å (methyl), 0.97 Å (methylene), and 0.98 Å (methanetriyl). The programs Mercury[54] and POV-Ray[55] were both used to prepare molecular graphics. A summary of the data collection and structure refinement parameters is provided in Table 1. CCDC reference numbers 2041839 and 2041840‡ contain the supplementary crystallographic data for this paper.

Table 1 Crystal data and details of the refinement parameters for the crystal structures **1** and **2**

Compound reference	**1**	**2**
Chemical formula	$C_{18}H_{24}Cl_2N_4Ru$	$C_{19}H_{26}Cl_2N_4Ru$
Formula mass	468.38	482.41
Crystal system	Orthorhombic	Triclinic
a/Å	16.2609(2)	7.6438(2)
b/Å	13.8629(1)	9.8677(3)
c/Å	17.0202(2)	14.0374(4)
α/°	90.00	78.921(2)
β/°	90.00	81.651(2)
γ/°	90.00	83.732(2)
Unit cell volume/Å^3	3836.75(7)	1024.44(5)
Temperature/K	293(2)	293(2)
Space group	*Pbca*	*P*$\bar{1}$
No. of formula units per unit cell, *Z*	8	2
Radiation type	MoKα	MoKα
Absorption coefficient, μ/mm^{-1}	1.104	1.036
No. of reflections measured	39 516	8849
No. of independent reflections	3916	4171
R_{int}	0.0612	0.0395
Final R_1 values ($I > 2\sigma(I)$)	0.0323[a]	0.0373[a]
Final w$R(F^2)$ values ($I > 2\sigma(I)$)	0.0838[b]	0.0962[b]
Final R_1 values (all data)	0.0361[a]	0.0403[a]
Final w$R(F^2)$ values (all data)	0.0875[b]	0.1002[b]
Goodness of fit on F^2	1.060	1.066

[a] $R_1 = \sum||F_o| - |F_c||/\sum|F_o|$. [b] $wR_2 = \{\sum[w(F_o^2 - F_c^2)^2]/\sum[w(F_o^2)^2]\}^{1/2}$.

Lipophilicity

The lipophilicity of ruthenium(II) complexes **1–3** and NAMI-A was determined using the shake-flask method.[56] Before experiments aqueous (0.9% v/v) sodium chloride and organic (1-octanol) phases were saturated for 1 week. All the ruthenium complexes were dissolved at a concentration of 0.30 mg mL^{-1} in 2.5 mL of the aqueous phase and an equal volume of the organic phase was added. Next, the solution was mechanically mixed in plastic tubes for 30 min, followed by centrifugation (6000 rpm, 15 min). After separation, the aqueous phases were analysed using UV–Vis spectroscopy to determine the amount of the compound in the measured phase. The absorption values before and after shaking were compared. The partition coefficient ($\log P_{o/w}$) for each compound was calculated based on the Lambert–Beer law to determine the $\log P_{o/w}$ values. For each complex, the procedure was repeated three times. Selected wavelengths for **1–3** and NAMI-A at which the absorbance maximum was observed, epsilon at the wavelength chosen and standard deviation for determining $\log P_{o/w}$ values are presented in Table S1.‡

Cell culture and compounds preparation

MCF-7 human breast cancer cell line was obtained from European Collection of Authenticated Cell Cultures (Salisbury, UK). MCF-7 cells were cultured in a complete RPMI 1640 medium containing 2 mM L-glutamine, heat-inactivated 10% fetal bovine serum (FBS), 100 μg mL^{-1} streptomycin and 100 IU mL^{-1} penicillin and non-essential amino acids (all compounds from Sigma-Aldrich, Darmstadt, Germany).

The human cervical cancer cell line (HeLa) was purchased from American Type Culture Collection (Manassas, VA, USA). HeLa cells were cultured in Dulbecco's modified Eagle's medium (DMEM; Corning, NY, USA) supplemented with 10% FBS, 2 mM L-glutamine (PAA Laboratories, Cölbe, Germany), and 50 μg mL^{-1} gentamicin (PAA Laboratories). L929 murine fibroblast cells (American Type Culture Collection) were cultured in RPMI 1640 medium containing 2 mM L-glutamine, 10% FBS, 100 IU mL^{-1} penicillin, and 100 μg mL^{-1} streptomycin. All cell lines were grown in 25 cm^2 cell culture flasks and the culture medium was changed every 2–3 days. The cells were passaged when reaching 70–80% confluency. All cultures were grown at 37 °C under a humidified atmosphere containing 5% CO_2 and 95% air.

During the preparation of complexes for tests one mg of the tested compounds was dissolved in 10 μL of the suitable solvent: the tested complexes and NAMI-A in a nuclease-free, steam sterilized, DEPC treated water (Carl Roth, Karlsruhe, Germany), cisplatin (Sigma-Aldrich) in the culture medium. Then, the solutions of compounds were diluted in a suitable culture medium and instantly added to the 96-well plates (100 μL per well). All tested compounds were freshly prepared for each experiment.

Cells were seeded on a standard tissue culture 96-well plates at an appropriate for each assay density and pre-incubated at 37 °C in 5% CO_2 for 24 h. Then, all tested cell lines were stimulated for 48 h with the complexes, NAMI-A or cisplatin in the final concentration range of 0.2–800 μM under the same conditions. The control cells were incubated alone in the growth culture medium. All experiments were repeated in triplicate.

The growth inhibition of mammalian cells was studied using macrophages for the three strains of *Leishmania* spp. and Vero cells for *T. cruzi*. J774.2 macrophages (European Collection of Cell Culture – ECACC – number 91051511), which were originally obtained from a tumour in a female BALB/c rat in 1968, were grown in a minimum essential medium (MEM) plus glutamine (2 mM) and supplemented with 20% inactivated fetal bovine serum (FBS). Vero cells (Flow) were grown in Roswell Park Memorial Institute medium (RPMI), which was supplemented with 10% inactivated fetal bovine serum. Both cell cultures were incubated in a humidified 95% air, 5% CO_2 atmosphere at 37 °C for several days. The compounds were tested at the concentration of 50, 100, 200 and 400 μM.

MTT assay for testing cell viability

3-(4,5-Dimethyl-2-thiazolyl)-2,5-diphenyl-2*H*-tetrazolium bromide (MTT; Sigma-Aldrich) assay was performed to evaluate the viability of the cell after the complexes, NAMI-A and cisplatin treatment. This colorimetric test detects the reduction of MTT by mitochondrial dehydrogenase to blue formazan product, which reflects the normal functioning of mitochondria and hence the metabolic rate of cells. For each experiment, 5×10^3 cells were seeded into 96-well culture plates in the complete culture medium. After stimulation, the cells were washed with PBS and 10 μL per well of MTT solution (5 mg mL^{-1} of MTT reagent in PBS) was added to each well. Culture plates were incubated at 37 °C for 3 h. Then, a formazan product formed by viable cells was dissolved in 100% DMSO. The optical density was measured at 570 nm (with a reference wavelength of 630 nm) using Synergy HT Multi-Mode Microplate Reader (BioTek Instruments, Winooski, VT, USA). The results were expressed as a percentage of control untreated cells, which was served as 100%. The 50% inhibitory concentrations (IC_{50}) were derived by a sigmoidal dose–response (variable slope) curve using GraphPad Prism 7.0 (GraphPad Software Inc., La Jolla, CA, USA). The following equation to model the data was selected: log(inhibitor) *vs.* normalized response – variable slope. Fits for the dose–response curves are presented in Fig. S1.‡

LDH assay for testing cell cytotoxicity

The leakage of lactate dehydrogenase (LDH) in the cells was determined using a CytoTox 96 non-radioactive cytotoxicity assay (Promega, Madison, WI, USA). This assay was used to assess cell membrane integrity. LDH is a stable cytosolic enzyme that is released upon cell lysis. Released LDH in culture supernatants is measured with an enzymatic assay, which results in the conversion of a tetrazolium salt (iodonitrotetrazolium violet; INT) into a red formazan product. The amount of color formed is proportional to the number of lysed cells.

The cells were seeded at a density of 5×10^3 per well into 96-well plates in the culture medium. After treatment, 50 μL of aliquots of supernatants were transferred to the new wells of 96-well plate and mixed with equal amounts of freshly prepared assay CytoTox 96 Reagent supported by the assay kit. The microtiter plate was incubated for 30 min at room temperature in the dark. The absorbance was measured at 490 nm using the Synergy HT Multi-Mode Microplate Reade. The complexes-mediated cytotoxicity was calculated according to the formula:

$$\%\ \text{cytotoxicity} = \text{experimental LDH release (OD490)} / \text{maximum LDH release (OD490)}$$

where the maximal release was obtained after lysis of the cells with a control solution (0.8% Triton X-100 served as 100%) provided by the manufacturer. All data were from three independent experiments with five wells for each experiment.

Fits for the dose–response curves are presented in Fig. S2.‡

Reactive oxygen species level measured using DCF-DA method

Intracellular formation of reactive oxygen species (ROS) was assessed using oxidation sensitive dye 2′,7′-dichlorofluorescin diacetate (DCF-DA; Sigma-Aldrich, Darmstadt, Germany) as a substrate. Cells were seeded in 96-well cell culture plates at a density of 1×10^4 (HeLa cells) or 25×10^3 (L929 and MCF-7 cells) in 200 μL of a complete growth medium. After pre-incubation, cells were washed twice with PBS and incubated with 20 μM DCFH-DA (200 μL per well) at 37 °C for 30 min in the dark. DCFH-DA solution was removed and the cells were washed again with PBS. Subsequently, the cells were treated with the various concentrations of the complexes, NAMI-A or cisplatin for 48 h. Finally, fluorescence was measured in a Synergy HT Multi-Mode Microplate Reader using excitation at 485 nm and emission at 528 nm. Blank wells contained the corresponding concentrations of the compounds without cells. All data were from three independent experiments with five wells for each concentration. The results were expressed as a percentage of control untreated cells (served as 100%).

Wound healing assay (scratch assay)

The wound healing assay (scratch assay) was used for evaluation of the effect of compounds (**1–3** and NAMI-A) on the HeLa cells, which were the most sensitive to a cytotoxic effect of the complexes among the all tested cell lines. The suspensions of cells were seeded in 12-well plates (0.1×10^6 cells per well) and incubated in DMEM medium containing 10% FBS until the culture reached 100% of confluence. Afterward, cell monolayers were mechanically scratched with a 10 μL pipette tip and unbound cells were removed by washing with PBS. The cells were then incubated with DMEM medium containing 2%

FBS and treated with the compounds at a concentration of 400 μM, which the most effectively inhibited cell growth. The control sample contained the cells and a standard medium without any active agents. Cell migration into the scratched region was recorded using the inverted microscope Leica DMi1 with a digital camera (Wetzlar, Germany). Cell migration at 0, 24 and 48 h were captured and wound closure distance was calculated by Image J software (National Institutes of Health, Bethesda, MD, USA). The scratch closure is expressed in percentage by the following formula:

$$\text{Scratch closure } (\%) = (D_0 - D_t)/D_0 \times 100\%$$

where D_0 is the scratch distance at 0 h and D_t is the scratch distance at the designated time.

All data were from three independent experiments, each with three measuring points. The results were expressed as a percentage of control untreated cells (served as 100%).

Statistical analysis

All values are reported as means ± standard error of the means (SEM) and were analyzed using analysis of variance followed by Bonferroni multiple comparisons test with the level of significance set at $p < 0.05$. Statistical analyses were performed with GraphPad Prism 7.0 (La Jolla, CA, USA).

All significant differences between L929 fibroblasts and the two cancer cell lines are marked in the figures with asterisks ($*p < 0.05$, $**p < 0.01$, $***p < 0.001$).

Antiparasitic studies

Promastigote forms of *L. infantum* (MCAN/ES/2001/UCM-10), *L. braziliensis* (MHOM/BR/1975/M2904) and epimastigote forms of *Trypanosoma cruzi* (IRHOD/CO/2008/SN3) were cultivated *in vitro* in medium trypanosome liquid (MTL) [Hank's balanced salt solution (HBSS) (Gibco), $NaHCO_3$, lactalbumin, yeast extract, bovine hemoglobin and antibiotics] with 10% inactive fetal bovine serum and were kept in an air atmosphere at 28 °C, in Roux flasks (Corning, USA) with a surface area of 75 cm^2, according to the methodology described by González *et al.*[57] The screening of extracellular forms of parasites was carried out using 24-well plates with MTL medium and 5×10^4 parasites per well. The compounds were tested at the concentration of 1, 10, 25 and 50 μM, prepared from mother aqueous solutions of the compounds, leaving some wells without drugs as control, and were incubated at 28 °C during 72 h before the parasite final count.

Alamar Blue assay for testing cell cytotoxicity

The cytotoxicity tests for macrophages and Vero cells were performed at the cell experiment unit in the "Centro de Instrumentación Científica" of the University of Granada, according to the methodology described below. The experiment was carried out in 96-well plates to be measured in the ELISA reader. First, the cells were sowed in a 96-well plate (2500 cells per well for macrophages and 3500 cells per well for Vero cells) to a volume of 100 μL per well and then were incubated at 37 °C with 5% CO_2 for 24 h. The complexes solutions were prepared in advance corresponding to the average growing cells (RPMI 10% FBS for Vero cells and MEM + Glut 20% FBS for macrophages) at double of the highest concentration to be tested. The solutions were performed in a sterile bath with the different channels, by adding 100 μL of complex solution or medium (only adding medium in the control wells) to the corresponding well. After that, the plate was incubated at 37 °C with 5% CO_2 for 48 h. Two days after, 20 μL of Alamar Blue dye (10% of the volume of the well) was added to each well and incubated at 37 °C with 5% CO_2 during another day. The whole incubation time once the products were added was 72 h, coinciding with the screening period to have comparable selectivity index (SI) results. Finally, the plate was read with an ELISA reader with Alamar Blue.

Kinetic measurements

Time-resolved spectra and the stopped-flow measurements were recorded on an SX20 Applied Photophysics spectrometer, equipped with a SX/PDADC diode-array detector (PDA) and a thermostatted SX/SQ sequential-mixing stopped-flow accessory. In the experiments, the concentration of ruthenium(II) was fixed at 0.1–0.5 mM. The measurements were performed in 100 mM phosphate-buffered solutions (OH^-, $H_2PO_4^-$, HPO_4^{2-}, PO_4^{3-}, Na^+). The other experimental conditions were as follows: T = 298 K, pH = 6.5–8.0, λ = 420 nm. The ruthenium compounds were dissolved in 200 mM NaCl before mixing with buffer solutions in stopped-flow accessory. Two fast hydrolytic processes could not be separated and both rate constants (k_{1obs}, k_{2obs}) were calculated from the two consecutive reaction scheme A → B → C and the non-linear least-squares fit to the two-exponential dependence of absorbance *vs.* time (t), $\text{Abs} = A_0 + A_1 \exp(-t/T_1) + A_2 \exp(-t/T_2)$, where $T_1 = 1/k_{1obs}$ and $T_2 = 1/k_{2obs}$. Kinetic data were analysed using dedicated acquisition and analysis Pro-Data SX software including Pro-Data instrument control software, Pro-Data Viewer and Pro-Data Converter. The reported rate constants are the mean values of at least four determinations. The relative standard errors of the pseudo-first-order rate constants for a single kinetic trace were *ca.* 0.5–1%.

Molecular docking

Molecular docking studies on compounds **1–3** and their diaqua derivatives have been performed using Vina[58] and Gold[59] programs. Iron instead of ruthenium has been used in Vina. Validation of using iron complexes as a proxy to ruthenium complexes is extensively described in the ESI.‡ In brief, using the literature data on a ruthenium complex (docked with aid of the Hex program) to an enzyme, we have shown that docking the corresponding iron complex yields identical results. We favor using iron for which parameters have been included in parametrization sets in the majority of docking programs. The density functional theory (DFT) calculations were carried out using the Gaussian16 program[60] with ωB97X-D functional[61,62] expressed in the def2-TZVP basis set.[63] The crystal structure of the DNA fragment (PDB ID: 1FYY[64]) long enough to allow studies of intercalation and

binding to the minor groove, and human serum albumin (PDB ID: 4F5S[65]) were retrieved from the protein data bank (http://www.rcsb.org/).[66] For blind docking, a rectangular box (Vina) and a sphere (Gold) containing the whole chain A of the enzyme has been used. Due to the known problems[67] with blind docking to DNA fragments in Vina, a smaller rectangular box that included base pairs neighboring the native ligand has been used. Similarly, spheres with 7.5 Å radius, centered either at the center of the natively intercalated ligand or moved 7 Å toward the groove have been used for docking in Gold. Two tautomeric forms of the HmtpO ligand, with proton on the nitrogen atom or oxygen atom, are possible for **3** (Fig. S6‡). We have optimized quantum-mechanically structures of both tautomers. In the case of the gas phase structures enol form has been found to be more stable by 2.3 kcal mol^{-1}. However, when the energy term from the continuum solvent model of water (SMD[68]) has been added the resulting difference changed to 9.0 kcal mol^{-1} in favor of the keto form (with the proton located on the nitrogen atom). Since the continuum solvent model does not fully incorporate interactions of the explicit solvent molecules with the solute, we consider these results as inconclusive regarding the preferred tautomeric form under experimental conditions. Therefore, we have used both of them (marked as $\mathbf{3_{NH}}$ and $\mathbf{3_{OH}}$) in docking studies. Chimera,[69] Mercury,[70] and GaussView[71] programs were used for visualization purposes.

Interaction with CT-DNA

The binding of the complexes **1–3** with polymeric CT-DNA was evaluated *via* CD spectroscopy. The solid DNA salt was dissolved in ultrapure water (18.2 MΩ) and left at 2–5 °C for 24 h to fully hydrate. The concentration of the DNA stock solution was determined spectroscopically, using the known molar extinction coefficient of CT-DNA at 258 nm, ε_{258} = 6600 M^{-1} cm^{-1}.[72] CD spectra were collected in 1 cm path length quartz cuvettes. All CT-DNA experiments involve 150 μM concentration of CT-DNA and a range of the metal complex (100 : 1, 25 : 1, 5 : 1, 1 : 1 for CT-DNA : Ru(II) complex) dissolved in water and phosphate buffer (10 mM, pH = 7.4). The CD spectra of these solutions were measured after 24 h of incubation at 37 °C.

Interaction with bovine serum albumin (BSA)

The interactions of the complexes **1–3** with BSA were studied by CD spectroscopy at 180–260 nm (intrinsic region; 0.2 cm path length quartz cuvette) and 300–600 nm (visible region; 1 cm path length quartz cuvette) in 10 mM phosphate buffer, pH = 7.4. Solid BSA was dissolved in ultrapure water (18.2 MΩ) and the resulting BSA stock solution was used freshly. All experiments involve 1.5 μM concentration of BSA (intrinsic region) and 150 μM BSA (visible region) and increasing concentrations of the Ru(II) complexes (1–12 eq. and 1–8 eq., respectively) dissolved in water. The CD spectra of these solutions were measured after 24 h of incubation at 37 °C.

Results and discussion

Synthesis and structural characterization

The synthesis of the new complexes **1–3** is based on the two-step reaction of ruthenium(III) chloride hydrate with α-terpinene in the first step followed by the reaction of Ru(II) dimer $[(\eta^6\text{-}p\text{-cym})RuCl_2]_2$ with the respective triazolopyrimidine derivative (tmtp, detp or HmtpO) in molar ratio 1 : 2 (Scheme 1). Complexes **1–3** were obtained in good (64% for **3**) to very good (83–90% for **1–2**) yield as air-stable powders. The presence of the two most characteristic bands in the IR spectra of **1–3**, at 1615–1640 cm^{-1} and 1527–1580 cm^{-1} respectively, which could be assigned to an overall pyrimidine and triazole ring vibration mode, confirms the formation of coordinated triazolopyrimidines. Moreover, this has been clearly confirmed by X-ray studies on **1** and **2** (suitable monocrystals were obtained by slow evaporation of the filtrate at r.t.). Furthermore, in view of the potential therapeutic use, an important aspect of the title ruthenium complexes is the confirmation that the structure is maintained in solution. Therefore, multinuclear magnetic resonance spectroscopy (^1H, ^{13}C, ^{15}N) was used (Fig. S7–S21‡) to determine the environment of the central atom and the ligand binding mode in **1–3**. Kinetic tests were also performed to determine the reactivity and stability of the complexes in buffered aqueous solutions. From an application point of view, it is important that these remain stable in biofluids or in the cytoplasm of cancer cells.

Kinetic studies

Under normal physiological conditions, the pH of blood and tissue is tightly controlled around pH 7.4. However, in diseased tissues such as the tumor microenvironment a local pH range from 5.5 to 7.0 is not uncommon.[73,74] The pH of cancer cells decreases as a result of anaerobic glycolysis, glutaminolysis, and ATP hydrolysis, in which hydrogen ions are formed and are accumulated in the cell, when, an increased H^+ ion production coincides with insufficient drainage by convective and/or diffusive transport of H^+ ions.[75,76] It is important to analyze in what chemical form the ruthenium compound reaches the tumor cells and what happens inside the diseased tissues. On the other hand, it is also important to determine whether the ruthenium compounds undergo similar changes inside healthy cells, where the pH is higher. This fact may influence its potential toxicity if more reactive forms are formed that can interact with various biomolecules in the cell. Therefore the kinetic stability of ruthenium(II) compounds with arene was examined spectrophotometrically in phosphate buffers ranging from pH 6.5 to 8 at 25 °C.

It was established that the reaction proceeds through two stages according to the scheme A → B → C (Fig. S22‡). The observed pseudo-first-order rate constants of both stages (k_{1obs} and k_{2obs}) are presented in Table 2. The reaction rate for all compounds tested does not change significantly. Therefore, no significant differences in the reactivity of these compounds could be observed.

Table 2 Pseudo-first-order rate constants for the hydrolysis of the ruthenium(II) complexes (k_{1obs} and k_{2obs}). Experimental conditions: [Ru^{II}] = 5×10^{-4} M, T = 298 K, λ = 420 nm

Complex	pH	k_{1obs} [s^{-1}]	k_{2obs} [s^{-1}]
[(η^6-*p*-cym)Ru(tmtp)Cl_2] (**1**)	8	0.188 ± 0.05	0.0270 ± 0.003
	7.5	0.199 ± 0.004	0.0319 ± 0.0006
	7	0.222 ± 0.01	0.0365 ± 0.0006
	6.5	0.186 ± 0.002	0.0399 ± 0.0002
[(η^6-*p*-cym)Ru(detp)Cl_2] (**2**)	8	0.175 ± 0.03	0.0201 ± 0.001
	7.5	0.212 ± 0.02	0.0257 ± 0.0009
	7	0.166 ± 0.01	0.0263 ± 0.001
	6.5	0.180 ± 0.01	0.0305 ± 0.0009
[(η^6-*p*-cym)Ru(HmtpO)Cl_2] (**3**)	8	0.126 ± 0.02	0.0178 ± 0.002
	7.5	0.166 ± 0.02	0.0195 ± 0.0006
	7	0.168 ± 0.001	0.0202 ± 0.0001
	6.5	0.199 ± 0.006	0.0235 ± 0.0001

Due to the strong electron-acceptor properties of arenes, their presence in the coordination sphere of ruthenium(II) compounds is an important factor influencing the reactivity of these complexes in solution. However, the presence of various triazolopyrimidine derivatives only has a secondary effect.

As the pH decreases, the rate constant for the first process is not changed, k_{1obs}, and a slight increase in the reaction rate for the second process, k_{2obs}, is observed for each of the compounds tested, suggesting that in more acidic solutions the reaction should proceed mostly *via* a spontaneous reaction path rather than according to the mechanism of a H^+-ion catalysed reaction. The two processes observed are associated with the dissociation of two chloride ions. In the visible range, spectral changes in the hydrolysis process of the ruthenium(II) compound (Fig. 1 and Fig. S23, S24‡), which is accompanied by a blue shift of the visible transition band towards higher energies, in both stages of the reaction, are consistent with dissociation of weak-field ligand (Cl^-) and association of the water molecule with the effect of the stronger field. In neutral solutions, at pH = 7, Ru(II) compounds hydrolyze within 100 s, forming diaqua derivatives. Arene compounds, like other organometallic compounds of ruthenium(II), are kinetically labile.[77] [(η^6-*p*-cym)Ru(tmtp)Cl_2] (**1**), with rate constants of 0.22 ± 0.01 s^{-1} and 0.0365 ± 0.0006 s^{-1} (pH = 7, Table 2) respectively, is more reactive than a chloride complex with triazolopyrimidine but without arene in its inner coordination sphere, *cis*,*fac*-[$RuCl_2$(dmso)$_3$(tmtp)], with a hydrolysis rate constant of 0.21×10^{-3} s^{-1}.[78] The value of the rate constant of complex **1** is three orders of magnitude higher than that observed for the latter. The water exchange reaction of [Ru(η^6-C_6H_6)(H_2O)$_3$]$^{2+}$ is also greatly labilized by π-acceptor spectator ligands and is attributed to the *trans* labilizing effect of the π-acid (η^6-C_6H_6). The [Ru(η^6-C_6H_6)(H_2O)$_3$]$^{2+}$ complex with rate constant of 11.5 s^{-1} (298 K)[79] is even two orders of magnitude more reactive than complexes **1**, **2** and **3**, whereas the cymene analogue,[80] [Ru(η^6-*p*-cym)(bpy)(H_2O)]$^{2+}$, shows similar lability (k_{ex} = 0.085 s^{-1}, 298 K) to the cymene complexes **1**, **2** and **3** with triazolopyrimidine (Table 2). Arene Ru(II) complexes **1**, **2**, and **3** are also more labile than [$RuCl_4$(py)(dmso)]$^-$ (AziRu) and some lipophilic Ru(III) complexes with liponucleoside modified pyridine, [$RuCl_4$(py-nucleolipid)(dmso)]$^-$ (ToThyRu), or lipoamino acid modified pyridine ligand, [$RuCl_4$(py-lipoamino acid)(dmso)]$^-$, in hydrolytic clevage of Cl^- ions. The half-life of 45 min, 90 min and 105 min for [$RuCl_4$(py)(dmso)]$^-$, [$RuCl_4$(py-nucleolipid)(dmso)]$^-$, and [$RuCl_4$(py-lipoamino acid)(dmso)]$^-$ are at least 3 order higher than the half-life $t_{1/2}$ (k_{1obs}) = 3 s, $t_{1/2}$ (k_{2obs}) = 19 s (pH = 7.0) for arene complex **1**.[81]

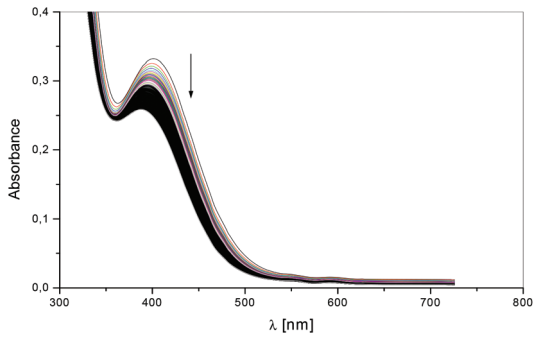

Fig. 1 Spectral changes observed during the base hydrolysis of the [(η^6-*p*-cym)Ru(tmtp)Cl_2] (**1**). Experimental conditions: [Ru^{II}] = 5×10^{-4} M, 100 mM phosphate buffer (OH^-, $H_2PO_4^-$, HPO_4^{2-}, PO_4^{3-}, Na^+), pH = 7, T = 298 K, t = 100 s, Δt = 0.2 s.

The products of the reaction were analysed by the ESI-MS and ESI-MS/MS in the negative ion mode and in the positive ion mode. The positive ion mode ESI mass spectra of the [(η^6-*p*-cym)Ru(tmtp)Cl_2] did not show molecular signal $[MH]^+$. The most intense signal was obtained for ion, formed after losing one chlorine atom at 433 *m*/*z* only in the mixture of ACN and aqueous solution. The mass spectra, simulated isotope distribution and the fragmentation spectra at 433 *m*/*z* are identical with the mass spectra of the $[C_{18}H_{24}N_4RuCl]^+$ cation, which means that ionization of these compounds took place *via* the loss of chloride ions (Fig. S25–S27‡). Nevertheless, it is difficult to distinguish whether this ion is a fragment of the product of hydrolysis without H_2O molecule or the starting complex, also because this signal does not appear in the aqueous solution in the presence of chloride. A very interesting signal was observed at 504 *m*/*z*. It was found that these compounds can exist as a dimer in the mixture of ACN and aqueous solution. The signal at 504 *m*/*z* corresponds to the [Ru_2(η^6-cym)$_2$Cl] fragment. This is probably not the second-generation product that appeared after the hydrolysis, since no second-order kinetics are observed in the reaction of these compounds in aqueous buffered solutions. The scan of its mass spectrum is provided in ESI (Fig. S28‡). According to literature, this is a common feature for half-sandwich Ru(II) complexes, where ruthenium is connected to the electronegative substituents.[82]

Crystal structures of 1 and 2

Determination of the crystal structures confirmed the formation of Ru(II) complexes of general formula [(η^6-*p*-cym)Ru(L)

Cl_2], whereby L = tmtp (for **1**) and detp (for **2**). These are closely related to previously reported complexes containing triazolopyrimidines such as 1,2,4-triazolo[1,5-*a*]pyrimidine (tp), 5,7-ditertbutyl-1,2,4,-triazolo[1,5-*a*]pyrimidine (dbtp), 5,7-dimethyl-1,2,4,-triazolo[1,5-*a*]pyrimidine (dmtp), 5-methyl-7-isobutyl-1,2,4,-triazolo[1,5-*a*]pyrimidine (ibmtp) and 5,7-diphenyl-1,2,4,-triazolo[1,5-*a*]pyrimidine (dptp), with crystal structures described for the complexes with the three latter ligands.[83] Comparing these with the crystal structures of **1** and **2** presented in this work, it is worth noting that all compounds containing two substituents in positions 5 and 7 of the fused rings crystallise in the centrosymmetric space group *P*1 of a triclinic system, whereas complex **1**, containing three methyl substituents on the bicyclic scaffold in positions 5,6,7 crystallises in the *Pbca* space group of an orthorombic system. Both novel Ru(II) complexes show the presence of one complex molecule in the asymmetric unit (Fig. 2). They adopt a typical three-legged piano-stool geometry with the legs formed by the 2 chloride ions and a nitrogen atom orginating from the triazolopyrimidine ligand. The C (orginating from η^6-arene)–Ru distances range from 2.177(2) to 2.205(3) Å and from 2.176(3) to 2.224(3) Å for **1** and **2** respectively. The angles Cg–Cl (Cg stands for the centroid of the *p*-cymene ring) of *ca.* 127° and Cg–N of *ca.* 132° correspond well with the values found for the previously reported compounds. The same holds true for the bond lengths (Table 3).

In general, the molecular structures of **1** and **2** are pretty much the same, as shown in Fig. S29,‡ depicting their overlay. This means that the dihedral angles between the planes of the *p*-cymene ligand and the triazolopyrymidines do not deviate much from one another, being 83.53(6)° in **1** and 88.40(7)° in **2**, respectively. The corresponding value for the three previously reported compounds was ranging from 83.07(13)° in the compound with ibmtp (CSD refcode: TUZROX) to 40.86(13)° in the compound with dptp (TUZRUD).

The differences in molecular packing, hydrogen bonds and π–π stacking in **1** and **2** are presented in ESI.‡

Table 3 Selected bond lengths [Å] and angles [°] for **1** and **2**

1		**2**	
Ru1–N3	2.123(2)	Ru1–N3	2.140(2)
Ru1–Cg	1.666(1)	Ru1–Cg	1.676(1)
Ru1–Cl2	2.4321(7)	Ru1–Cl2	2.4213(8)
Ru1–Cl1	2.4397(6)	Ru1–Cl1	2.4283(8)
N3–Ru1–Cl2	82.17(6)	N3–Ru1–Cl2	83.99(7)
N3–Ru1–Cl1	86.20(5)	N3–Ru1–Cl1	83.38(7)
Cl2–Ru1–Cl1	88.19(2)	Cl2–Ru1–Cl1	88.05(3)
Cg–Ru1–Cl1	125.76(4)	Cg–Ru1–Cl1	127.03(5)
Cg–Ru1–Cl2	127.86(4)	Cg–Ru1–Cl2	126.48(5)
Cg–Ru1–N3	131.58(6)	Cg–Ru1–N3	132.47(8)

In vitro cytotoxicity

The cytotoxic effect of the tested compounds on L929 murine fibroblasts and two cancer cell lines, human breast cancer cell line (MCF-7) and human cervical cancer cell line (HeLa), was evaluated using two different assays. The cell viability was assessed by the MTT test, whereas the level of cell death was determined by measuring lactate dehydrogenase (LDH) leakage. As shown in Fig. 3, stimulation with all tested compounds decreased the viability of fibroblasts as well as cancer cells in a dose-dependent manner. Importantly, all tested complexes induced higher cytotoxicity against cancer cells in comparison with L929 fibroblasts. This effect was observed for all concentrations of the tested complexes, except for the cancer cells stimulated with [(η^6-*p*-cym)Ru(detp)Cl_2] (**2**) at a concentration of 0.2 μM. The cytotoxicity induced by the complexes was higher compared to NAMI-A, which is potent, antimetastatic ruthenium(III)-based drug tested in clinical trials. Moreover, only at the highest concentration used, NAMI-A showed a significantly lower cytotoxic effect on normal fibroblasts than on cancer cells.

The LDH release assay supports the results of the MTT test. As compared with the positive control (cells treated with Triton X-100 solution), L929 fibroblasts, as well as the cancer cells stimulated with all tested compounds, showed an increased LDH leakage in a concentration-dependent manner. However, both cancer cell lines stimulated with the tested complexes **1–3** released a greater amount of LDH compared to L929 fibroblasts. This effect was also observed when both cancer cell lines were treated with cisplatin, but only at concentrations of 0.2, 20 and 400 μM, as well as when HeLa cells were stimulated

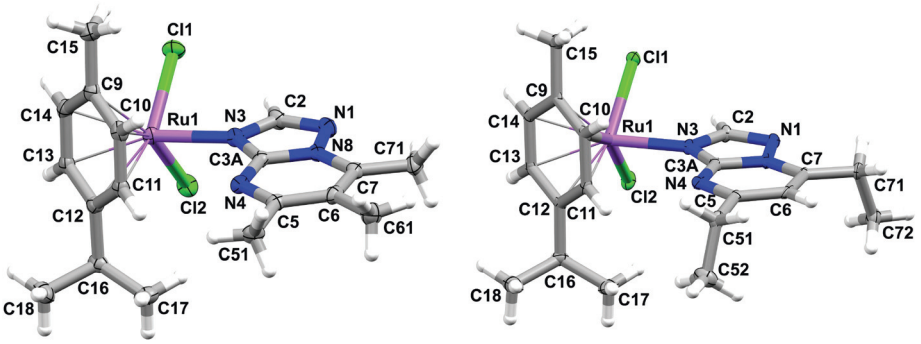

Fig. 2 Molecular structures of [(η^6-*p*-cym)Ru(tmtp)Cl_2] (**1**) (left) and [(η^6-*p*-cym)Ru(detp)Cl_2] (**2**) (right); atomic displacement plots shown with 50% probability.

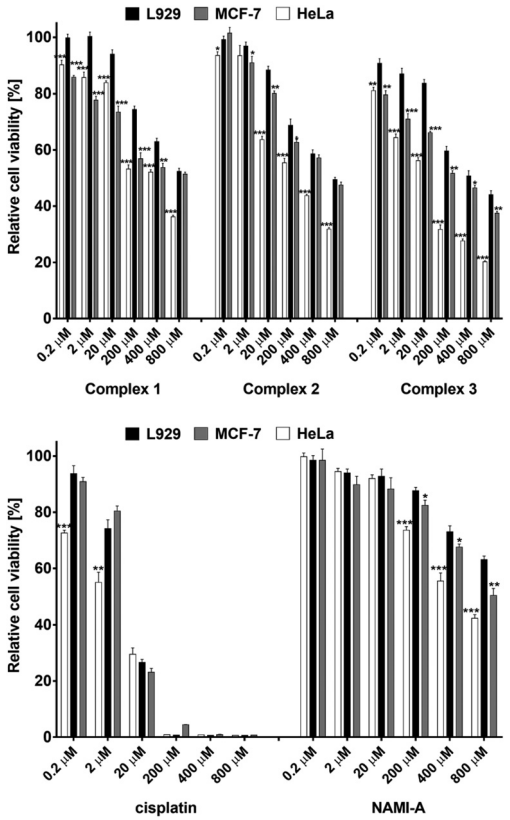

Fig. 3 Dose-dependent effect of the tested compounds on the viability of L929 compared to MCF-7 and HeLa cells.

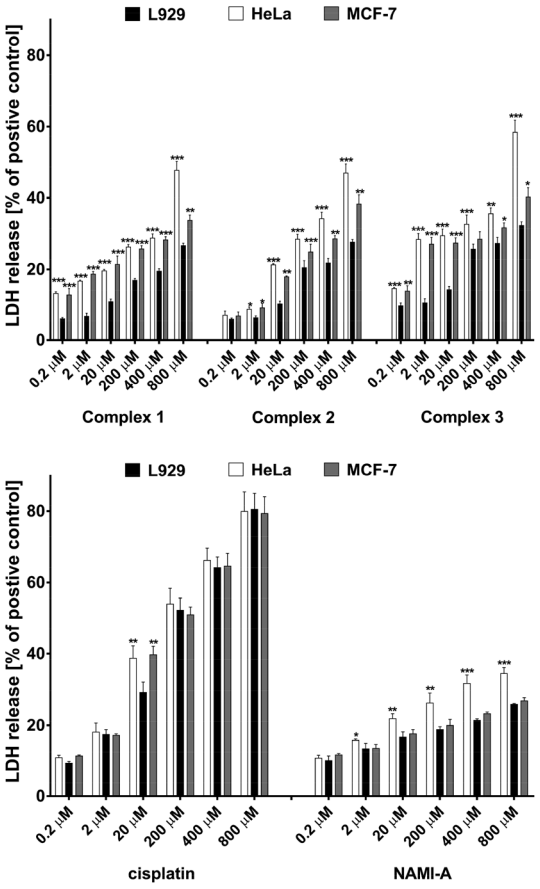

Fig. 4 Analysis of lactate dehydrogenase (LDH) release from MCF-7, HeLa and L929 cells stimulated with different concentrations of the tested compounds for 48 h.

with NAMI-A. The highest level of LDH release was observed for cells treated with cisplatin (Fig. 4).

The half inhibitory concentrations (IC_{50}) calculated based on the results from the MTT assay provide more detailed information about the cytotoxicity of the tested complexes (Table 4). These results show that [(η^6-*p*-cym)Ru(HmtpO)Cl_2] (**3**) inhibited MCF-7 and HeLa cancer cell growth with the highest anticancer efficiency (IC_{50} = 153 μM and 18 μM, respectively) of the newly obtained complexes **1–3**. In contrast, the lowest cytotoxicity was observed for MCF-7 and HeLa cancer cells stimulated with [(η^6-*p*-cym)Ru(tmtp)Cl_2] (**1**) (IC_{50} = 716 μM and 302 μM, respectively). Importantly, all tested complexes demonstrated higher cytotoxicity against both cancer cell lines in comparison with L929 normal fibroblasts (IC_{50} > 800 μM for **1**, 774 μM for **2** and 453 μM for **3**), but showed a lower inhibitory effect on cancer cell growth than cisplatin (IC_{50} = 8.0 μM for MCF-7 cells and IC_{50} = 2.1 μM for HeLa cells, respectively). Among all tested compounds, NAMI-A showed the weakest cytotoxic properties against all cell lines.

These significant differences in the activity of ruthenium-based complexes correlate with the lipophilicity of the molecules, with the most lipophilic complex **3** found to be the most active within **1–3** (Fig. 5). In theory, such log *P* values can constitute optimal values for passive drug absorption,[84,85] because log *P* values between 0 and 3 allow drug molecules to be lipophilic enough to partition into the lipid bilayer and hydrophilic enough to partition back to the aqueous environment of the cell.[86] The correlation of lpophilicity and *in vitro* cytotoxicity for ruthenium(II) complexes of type [(η^6-*p*-cym)Ru(N)Cl_2], where N = triazolopyrimidine derivatives, has already been observed in our previous studies.[83] Differences in cell lines tested and the lack of toxicity data for previously obtained compounds makes a direct comparison with **1–3** difficult. However, for the most cytotoxic [(η^6-*p*-cym)Ru(dptp)Cl_2], where dptp is 6,7-diphenyl-1,2,4-triazolo[1,5-*a*]pyrimidine, the IC_{50}

Table 4 IC_{50} values for **1–3**, NAMI-A and cisplatin against MCF-7 and HeLa cancer cell lines and L929 normal fibroblasts determined after 72 h of incubation by MTT assay

	IC_{50} (μM)		
Compound	MCF-7	HeLa	L929
[(η^6-*p*-cym)Ru(tmtp)Cl_2] (**1**)	716 ± 50	302 ± 8	>800
[(η^6-*p*-cym)Ru(detp)Cl_2] (**2**)	655 ± 84	167 ± 10	774 ± 36
[(η^6-*p*-cym)Ru(HmtpO)Cl_2] (**3**)	153 ± 19	18 ± 1	453 ± 63
NAMI-A	>800	599 ± 17	>800
Cisplatin	8.0 ± 0.4	2.1 ± 0.3	7.1 ± 1.1

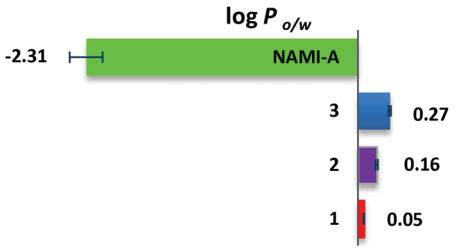

Fig. 5 The results of the log $P_{o/w}$ determination for **1–3** and NAMI-A in aqueous (0.9% w/v) sodium chloride and organic (1-octanol) phases.

values were 34.9 μM against T47D and 83.1 μM against A549, while for cisplatin the IC_{50} values were 8.2 μM and 8.4 μM, respectively.[83] On the other hand, it is known from various literature studies[21] that several ruthenium(II)-arene compounds, for example, the RAPTA complexes mentioned in the introduction, generally exhibit low cytotoxicity *in vitro* while being significantly antimetastatic *in vivo*.[22–24]

In view of these literature data, the presented *in vitro* cytotoxicity results against HeLa for **3**, combined with the much lower toxicity (64-fold) against normal cells than cisplatin, could be considered favorable.

Effect on reactive oxygen species (ROS) production in cells

To assess the capacity of the tested compounds to generate intracellular reactive oxygen species (ROS), L929 fibroblasts, as well as both cancer cell lines, were stained with 2′,7′-dichlorofluorescein diacetate (DCFH-DA) followed by stimulation with different concentrations of the compounds. As shown in Fig. 6, all tested complexes significantly increased ROS production in a concentration-dependent manner, though inducing less ROS generation (from about 1.9 to 2.5-fold increase for the highest concentration of the complexes) in comparison with cisplatin (about 4.0-fold increase for all tested cell lines stimulated with cisplatin at the highest concentration). Importantly, both cancer cell lines were more sensitive to the treatment and released a greater amount of ROS than L929 fibroblasts.

Antimigratory activity of the complexes

To investigate the antimetastatic activity of the complexes, a wound healing scratch assay was performed to estimate cell migration and repair ability. The degree of healing reflects the inhibitory effect of drugs on the migration ability of tumor cells. As shown in Fig. 7, HeLa cells treated with all tested complexes showed a lower percentage of scratch closure than unstimulated cells, both after 24 and 48 h of treatment. Among the tested complexes, [(η^6-*p*-cym)Ru(HmtpO)Cl_2] (**3**) induced the strongest inhibition of scratch closure (12.1 ± 1.1% and 28.6 ± 4.2%), whereas the highest percentage of scratch closure was observed for cells stimulated with [(η^6-*p*-cym)Ru(tmtp)Cl_2] (**1**) (34.4 ± 3.8% and 60.7 ± 5.6%) after 24 and 48 h, respectively. At the same time, for HeLa cells treated with NAMI-A, the percentage of scratch closure was 18.9 ± 2.1% and 27.6 ± 4.4%, respectively.

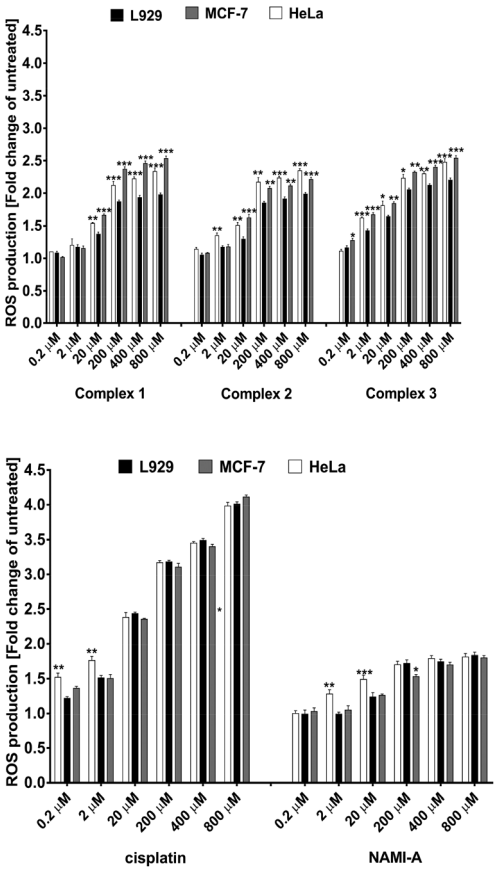

Fig. 6 Dose-dependent effect of the tested compounds on the levels of reactive oxygen species (ROS) in human MCF-7, HeLa and L929 cells.

Docking to serum albumin

Human serum albumin is a major circulatory protein with a binding affinity towards many endogenous and exogenous compounds, such as drugs in the blood. Thus, it was interesting to investigate the binding modes of **1–3** to BSA. Initially, the Vina docking program was employed. However, blind docking resulted in numerous possible binding sites with no clear preference, neither on the basis of the best score nor on the cluster population. The obtained sites are presented in Fig. 8a. Similar results were obtained with Hex (in agreement with literature data, see Fig. S22 of ref. 87). In contrast, the docking results using Gold yielded a single binding site, corresponding to the site reported in literature[87] (described in the ESI‡). We, therefore, decided to carry out the docking studies using this software package.

Table 5 summarizes the obtained results, with the strongest interactions between the complex and the enzyme predicted for **2**. It is, however, interesting to note that the best pose obtained for $\mathbf{3_{NH}}$ occupies a different position than all poses obtained for this as well as the other complexes, as illustrated in Fig. 8b.

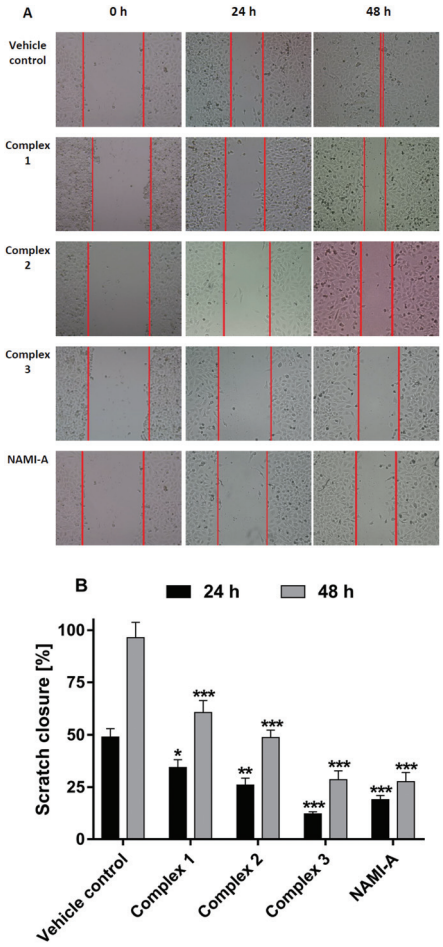

Fig. 7 Inhibitory effect of the complexes on the HeLa cell migration detected by a wound healing assay. HeLa cells were treated with the tested complexes and NAMI-A at a concentration of 400 μM. (A) Representative images at 0, 24 and 48 h of treatment with the compounds (magnification: ×40; scale bar: 50 μm). The boundaries of the scratched wounds were determined by the red lines. (B) Quantitative closure (%) measured using ImageJ software. The results were expressed as percentage of the control untreated cells. Asterisks show significant differences between the control cells and the cells stimulated with compounds (*$p < 0.05$, **$p < 0.01$, ***$p < 0.001$).

Table 5 Goldscore fitness scores[a] for the best poses in docking of studied dichloride and diaqua* complexes

		DNA	
Complex	BSA	Intercalation	Binding in minor groove
1	42.4	61.5	41.8
	43.0*		
2	51.0	65.2	44.2
	47.6	62.6*	43.1*
$\mathbf{3_{NH}}$ [b]	43.6	59.0	41.9
	41.2*		
$\mathbf{3_{OH}}$	43.0	56.8	44.7
	37.9*		

[a] Goldscore function takes into account hydrogen bonding, van der Waals and metal interactions, and ligand torsion strain. The higher the score, the better the complex fits the protein. [b] $\mathbf{3_{NH}}$ corresponds to complex **3** containing the keto form and $\mathbf{3_{OH}}$ the enol form of HmtpO (Fig. S6‡).

The binding site of $\mathbf{3_{NH}}$ is above (as defined by the view of the enzyme in figures used throughout this article) the binding site to which other complexes exhibit preferential binding. It involves both hydrophobic and hydrophilic residues Arg 194, Leu 197, Arg 198, Ser 201, Ala 209, Leu 210, Trp 213, Val 342, Ser 343, Leu 346, Asp 450, Ser 453, Leu 454, and Leu 480. A close-up of this site is provided in Fig. 8c.

Taking into account the fast hydrolysis time of **1–3**, docking of diaqua complexes to BSA and comparing the results seemed reasonable. This was done successfully and the results are very close to those of dichloride complexes (Table 5).

Docking to DNA

As DNA is the primary target of many anticancer agents, understanding the interactions between **1–3** and DNA by means of molecular docking could provide valuable information. The DNA (PDB ID: 1FYY) model used in the binding studies of complexes **1–3** allowed for elucidation of both typical modes of interaction, intercalation, and binding to the minor groove. It was revealed that in this case intercalation, which involves two A–T pairs, is much stronger than a binding

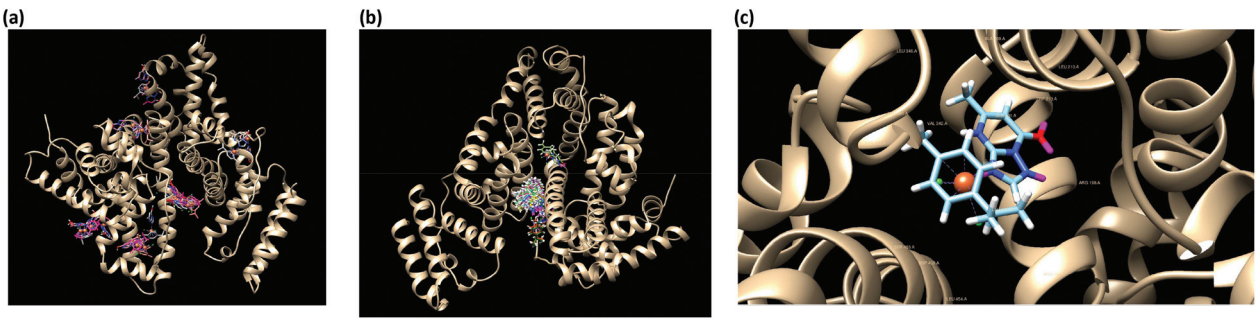

Fig. 8 (a) Results of blind docking of **1** to BSA using Vina; (b) poses obtained for studied complexes docked to BSA; (c) new binding site of BSA with bound $\mathbf{3_{NH}}$.

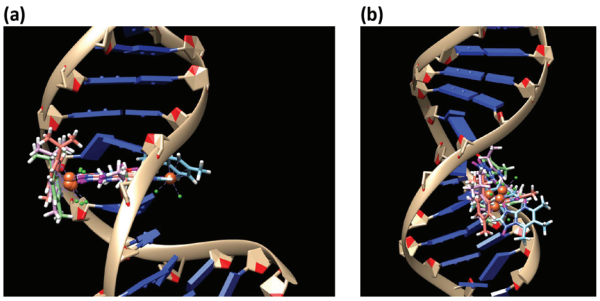

Fig. 9 Best poses of intercalation (a) and binding to the minor groove (b) for all complexes studied in docking to DNA.

in the groove, which, on the contrary, concerns two C–G pairs. While intercalation involves, as expected, π-stacking of the triazole-based ligands, no specific interactions have been identified for the binding in the minor groove and it could thus be assumed that the binding is governed solely by electrostatic interactions. Same as for the BSA binding, complex **2** exhibits the strongest intercalation affinity to DNA (Table 5). Binding of **3**, this time in the enol form, again exhibits a different orientation than the other complexes, with binding on the other side of the helix (illustrated in Fig. 9a), which may lead to different biological effects. Whereas $\mathbf{3_{OH}}$ intercalation is the weakest, binding of this complex in the minor groove has been found to be the strongest, which might be the result of the closer position of the metal to the receptor compared to the other complexes (see Fig. 9b).

Docking to DNA of diaqua derivatives of **2** also confirms that hydrolysis does not affect the previously obtained results (Table 5).

Interaction with biomolecules

To rationalize the observed during theoretical studies binding affinities of **1–3** with the target DNA and BSA CD spectral analysis for incubated biomolecules in the presence of **1–3** was performed. Circular dichroism provides valuable information on the binding mode of metal complexes with DNA[88] and can confirm M-protein interactions.[89–91]

In Fig. 10a, the CD spectrum of free DNA has a positive peak at approximately 278 nm and a negative peak at 247 nm, which corresponds to B-DNA. These bands are caused by stacking interactions between the bases and the helical supra-structure of the polynucleotide that provides an asymmetric environment for the bases.[92] By keeping the concentration of CT-DNA constant but varying the concentration of **1–3** (from 100 : 1 to 5 : 1 for CT-DNA : Ru complex) both positive and negative bands show marginal changes (represented by **2** in Fig. 10a and Fig. S30, S31‡), implying a non-intercalative mode of interaction between DNA and the Ru(II) complex. According to the literature data, little or no perturbation in the base stacking and helicity bands suggests simple groove binding or electrostatic interactions with the complex.[90] On the other hand, an increase in the concentration of **1–3** (1 : 1 molar ratio for CT-DNA : Ru complex) results in major perturbations in the

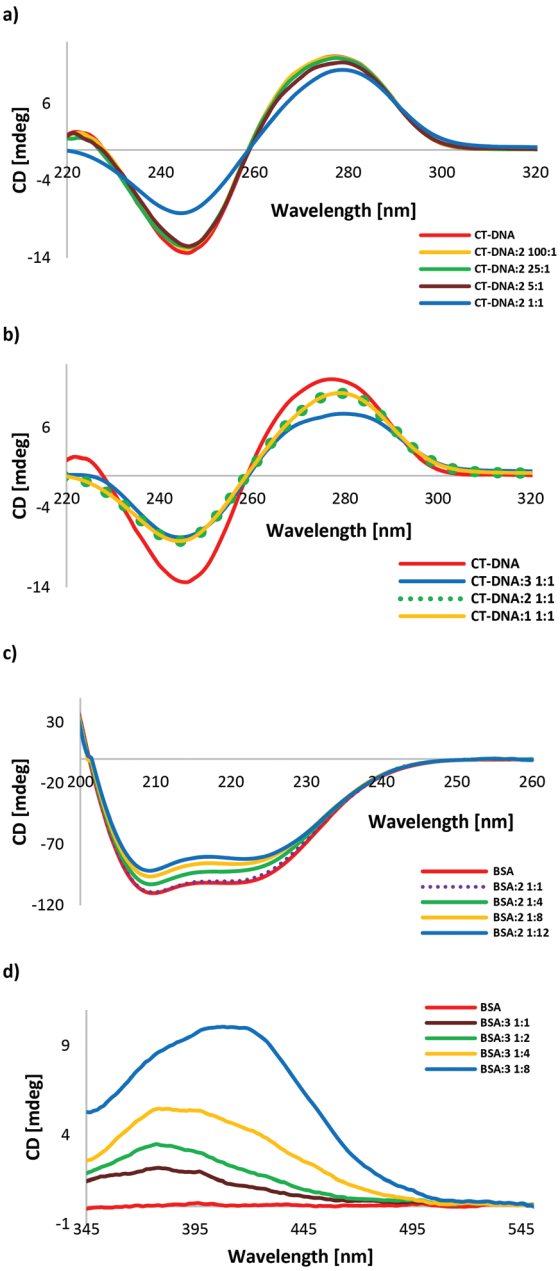

Fig. 10 CD spectra of: (a) CT-DNA (150 μM) after incubation with increasing concentrations of **2**; (b) comparison of CD spectra for CT-DNA after incubation with **1**, **2** and **3** at the highest tested concentration; (c) BSA (1.5 μM) after incubation with increasing concentrations of **2**; (d) BSA (150 μM) after incubation with increasing concentrations of **2**. Incubation time = 24 h, T = 37 °C, 10 mM phosphate buffer (pH = 7.4).

CD spectra (Fig. 10b) thus the presence of complexes significantly affects the base stacking of CT-DNA. These changes in the CD spectra for **1** and **2** are similar (Fig. 10b) and it may indicate intercalation between the base pairs. However, the most significant changes in the CD spectra are observed for **3** (Fig. 10b) for which molecular docking indicates that binding in the minor groove is the strongest.

The CD spectra of BSA (Fig. 10c) exhibit in the intrinsic region (180–260 nm) two negative bands at 209 and 220 nm, characteristic of right-handed α-helices.[93] Interaction of complexes **1–3** with BSA led to a similar reduction in the intensity of both bands (represented by **2** in Fig. 10c and Fig. S32, S33‡). Nevertheless, the spectra with or without the complex are basically similar in shape, suggesting that the α-helix remains the predominant conformation of BSA in this system. Changes were also monitored in the visible region of the CD spectrum. The free protein shows no signals in this region; however, wide bands appear after incubation with **1–3** (represented by **3** in Fig. 10d and Fig. S34, S35‡). These bands are a typical consequence of optical activity associated with d–d transitions of the metal atom upon interaction with the protein[94] and constitute unambiguous proof of a modification in the coordination sphere of the metal, thus confirming a Ru–protein interaction, most likely of a covalent nature. The band maximum is formed at higher concentration of the complex at about 379 nm. However, for complex **3** at a ratio of 1 : 8 the band maximum shifts (Fig. S36‡). By the correlation with the docking data, it can be related to a different binding site of $\mathbf{3_{NH}}$.

It is worth noting that in our intensive studies on the interaction of BSA with triazolopyrimidine Ru(III) and Ru(II) complexes of the type $[RuCl_3L_3]$, $[RuCl_3L_2(H_2O)]$ and $[RuCl_3L_2(dmso)]$,[95–97] $[RuCl_2(dmso)_2L_2]$ and $[RuCl_2(dmso)_3L]$,[98] where L = triazolopyrimidine analogues including tmtp, detp and HmtpO, lack of adduct formation with albumin was observed. Apparently, the presence of the arene and piano-stool geometry of Ru(II) complexes with these N-donor ligands promotes bonding of **1–3** with BSA.

In vitro antiparasitic activity

Encouraged by the interesting properties and biological activity of the complexes, we decided to check the antiparasitic activity of **1–3** against three strains of *Leishmania* spp. and *Trypanosoma cruzi* and compare with selected commercial drugs (Glucantime and Benznidazole, respectively) (Table 6).

The results show that the newly synthesized complexes **1–3** are very promising candidates and can compete with commercial antiparasitic drugs. Practically in every case, their leishmanicidal and trypanosomicidal efficacies significantly exceed that of the drugs and particularly, they are much less toxic against host cells. Similarly to the *in vitro* cytotoxicity studies, the most lipophilic complex **3** showed the highest activity (Table 6) against *T. cruzi* and *L. braziliensis* (IC_{50} < 1 μM) while against *L. infantum*, **2** is the most active (IC_{50} < 1 μM). From analysis of these results, toxicity data as well as selectivity index, it can be concluded that, to the best of our knowledge, **2** and **3** belong to the group of the most promising representatives of antiparasitic metal complexes with such N-donor ligands, making them excellent candidates for further studies, both *in vitro* and *in vivo*.

From previously reported triazolopyrimidine complexes displaying *in vitro* antiparasitic properties, other outstanding representatives are dinuclear silver complexes containing 5,7-dimethyl-1,2,4-triazolo[1,5-*a*]pyrimidine (dmtp),[38] such as $[Ag_2(dmtp)_3]_2$-$[Ag_2(dmtp)_2](BF_4)_6(H_2O)_2$, $[Ag_2(dmtp)_2(ClO_4)_2][Ag_2(dmtp)_2(H_2O)_2](ClO_4)_2$, and $[Ag_2(dmtp)_2(NO_3)_2]$, with IC_{50} values below 1 μM against all these strains. However, taking into account selectivity, only one of these compounds has parameters as remarkable as **2** and **3**. Of the Ru(II) and Ru(III) complexes with triazolopyrimidines tested so far, the most active was *cis*,*fac*-$[RuCl_2(dmso)_3(tmtp)]$, with an IC_{50} equal to 31.0 μM against *L. infantum* and 9.2 μM against *L. braziliensis*.[78] Towards *T. cruzi*, *fac*,*cis*-$[RuCl_3(H_2O)(tmtp)_2]$ was the most active (IC_{50} = 32.4 μM). A structural comparison of **1–3** and *cis*,*fac*-$[RuCl_2(dmso)_3(tmtp)]$ suggests that modification of the coordination sphere of the Ru(II) complex, by introducing the arene ligand instead of dmso near the triazolopyrimidine, is preferred, as this significantly affects the lipophilicity (for *cis*,*fac*-$[RuCl_2(dmso)_3(tmtp)]$, $\log P = -0.33$).

Comparison of the results obtained for complexes **1–3** with other published ruthenium complexes tested against the same strains would help to put the data in perspective. Ru-CTZ compounds, (where CTZ = clotrimazole) reported by Martínez *et al.*[42] were evaluated against *T. cruzi* with most of the Ru-CTZ family members showing appreciable antiparasitic effects (LD_{50} values in the range of 0.1–7.7 μM), similar to **2–3**. However, the results obtained for Ru-CTZ reveal toxicity on human osteoblasts, indicating that only one compound, [Ru(η^6-*p*-cymene)Cl_2(CTZ)], an analogue of **1–3** with a different N-donor ligand, does not display any appreciable toxicity

Table 6 *In vitro* activity of **1–3** against promastigote forms of *Leishmania* spp., epimastigote forms of *Trypanosoma cruzi*, J774.2 macrophages and Vero cells after 72 h of incubation at 37 °C

	IC_{50} [a] (μM)					SI[b]		
Compounds	*L. infantum*	*L. braziliensis*	*T. cruzi*	Macrophages J774.2	Vero cells	*L. infantum*	*L. braziliensis*	*T. cruzi*
Glucantime®	18.0 ± 0.6	25.6 ± 1.6	—	15.2 ± 1.3	—	0.8	0.6	—
Benznidazole®	—	—	15.2 ± 1.3	—	13.6 ± 0.9	—	—	0.9
[(η^6-*p*-cym)Ru(tmtp)Cl_2] (**1**)	28.0 ± 2.2	10.3 ± 0.8	18.6 ± 1.5	223.3 ± 17.9	>1000	8	22	>54
[(η^6-*p*-cym)Ru(detp)Cl_2] (**2**)	<1	1.3 ± 0.1	7.3 ± 0.6	292.5 ± 23.4	>1000	>293	225	>137
[(η^6-*p*-cym)Ru(HmtpO)Cl_2] (**3**)	8.2 ± 0.7	<1	<1	>1000	>1000	>122	>1000	>1000

[a] The concentration required to obtain 50% inhibition, calculated through a linear regression analysis from the K_c values at the concentrations employed (1, 10, 25, 50, 100 μM for promastigote forms of *Leishmania* spp., epimastigote forms of *Trypanosoma cruzi* and 50, 100, 200, 400 μM for host cells). [b] Selectivity index = IC_{50} against Vero cells or J774.2 macrophages/IC_{50} parasite (promastigote or epimastigote forms).

towards human osteoblasts at concentrations up to 7.5 μM, whereas other Ru(II) complexes containing CTZ showed lower IC_{50} values against normal cells in the range of 0.5–6.6 μM. Therefore, the toxicity results (IC_{50} ranging from 223 up to >1000 μM) obtained for **1–3** clearly demonstrate the favourable effect of triazolopyrimidines (Table 6).

Conclusions

Three new organometallic Ru(II) complexes of general formula $[(\eta^6\text{-}p\text{-cym})Ru(L)Cl_2]$, with L = purine analogs (triazolopyrimidines), possessing a piano-stool geometry, have been synthesized and structurally characterized by different techniques. *In vitro* studies revealed significantly lower *in vitro* cytotoxicity against HeLa and MCF-7 compared to cisplatin. The highest anticancer potential of newly synthesized **1–3** has the most lipophilic complex, namely, $[(\eta^6\text{-}p\text{-cym})Ru(HmtpO)Cl_2]$ (**3**) against HeLa cells, which is 7-fold more selective in comparison to cisplatin. The IC_{50} value for **3** against HeLa (18 μM) is remarkably lower than for **1** and **2** (IC_{50} = 302 μM and 167 μM, respectively). All these data indicate how the type of substituent in the 1,2,4-triazolo[1,5-*a*]pyrimidine core can affect the *in vitro* cytotoxicity. This difference in substituents at the ring has not significantly affected ROS generation since all tested complexes significantly increased ROS production in a dose-dependent manner. Likewise, the presence of various triazolopyrimidine derivatives has a secondary significance influencing the reactivity of these complexes in solution. However, molecular docking studies clearly indicate that different biological effects of **3** may be due to differences in binding sites with DNA and BSA. Importantly, docking results can correlate with experimental ones that suggested intercalation and groove binding as a mode of interaction of **1–3** with CT-DNA. Two characteristic for BSA ranges observed in CD spectra indicate that **1–3** also interact with albumin. The α-helix remains the predominant conformation of BSA in this system, however, there is evidence of adduct formation with BSA.

According to literature data, Ru(II) complexes with three-legged piano-stool geometry exhibit higher antimetastatic properties than *in vitro* cytotoxicity and we have actually confirmed this for **1–3** in a wound healing assay. The best candidate which can compete with NAMI-A is $[(\eta^6\text{-}p\text{-cym})Ru(HmtpO)Cl_2]$ (**3**).

Further investigations on the aspect of potential biological use of **1–3** revealed their high antiparasitic properties against *L. infantum*, *L. braziliensis* and *Trypanosoma Cruzi*. This first *in vitro* screening shows that the compounds are very promising in this regard. Their IC_{50} values and selectivity indices clearly warrant further studies.

Conflicts of interest

There are no conflicts to declare.

Acknowledgements

We would like to thank the student Aleksandra Ciepielewska from the Faculty of Chemistry, University of Wrocław for her assistance during the synthetic part.

Notes and references

1 M. Markman, *Expert Opin. Drug Saf.*, 2003, **2**, 597.
2 P. C. Bruijnincx and P. J. Sadler, *Curr. Opin. Chem. Biol.*, 2008, **12**, 197.
3 S. van Zutphen and J. Reedijk, *Coord. Chem. Rev.*, 2005, **249**, 2845.
4 Y. K. Yan, M. Melchart, A. Habtemariam and P. J. Sadler, *Chem. Commun.*, 2005, **38**, 4764.
5 M. Pala, U. Nandib and D. Mukherjee, *Eur. J. Med. Chem.*, 2018, **25**, 419.
6 R. Trondl, P. Heffeter, C. R. Kowol, M. A. Jakupec, W. Berger and B. K. Keppler, *Chem. Sci.*, 2014, **5**, 2925.
7 E. Alessio and L. Messori, *Molecules*, 2019, **24**, 1995.
8 C. Riccardi, D. Musumeci, M. Trifuoggi, C. Irace, L. Paduano and D. Montesarchio, *Pharmaceuticals*, 2019, **12**, 146.
9 J. M. Rademaker-Lakhai, D. van den Bongard, D. Pluim, J. H. Beijnen and J. H. M. Schellens, *Clin. Cancer Res.*, 2004, **10**, 3717.
10 C. G. Hartinger, M. A. Jakupec, S. Zorbas-Seifried, M. Groessl, A. Egger, W. Berger, H. Zorbas, P. J. Dyson and B. K. Keppler, *Chem. Biodiversity*, 2008, **5**, 2140.
11 L. S. Flocke, R. Trondl, M. A. Jakupec and B. K. Keppler, *Invest. New Drugs*, 2016, **34**, 261.
12 M. J. Clarke, S. Bitler, D. Rennert, M. Buchbinder and A. D. Kelman, *J. Inorg. Biochem.*, 1980, **12**, 79.
13 M. A. Jakupec, E. Reisner, A. Eichinger, M. Pongratz, V. B. Arion, M. Galanski, C. G. Hartinger and B. K. Keppler, *J. Med. Chem.*, 2005, **48**, 2831.
14 Y. K. Yan, M. Melchart, A. Habtemariam and P. J. Sadler, *Chem. Commun.*, 2005, 4764.
15 A. Bergamo and G. Sava, *Dalton Trans.*, 2011, **40**, 7817.
16 S. Hairat and M. Zaki, *J. Organomet. Chem.*, 2021, **937**, 121732.
17 A. A. Nazarov, Ch. G. Hartinger and P. J. Dyson, *J. Organomet. Chem.*, 2014, **751**, 251.
18 L. D. Dale, J. H. Tocher, T. M. Dyson, D. I. Edwards and D. A. Tocher, *Anticancer Drug Des.*, 1992, **7**, 3.
19 S. J. Dougan and P. J. Sadler, *Chimia*, 2007, **61**, 704.
20 P. J. Dyson, *Chimia*, 2007, **61**, 698.
21 W. H. Ang, A. Casini, G. Sava and P. J. Dyson, *J. Organomet. Chem.*, 2011, **696**, 989.
22 W. H. Ang, E. Daldini, C. Scolaro, R. Scopelliti, L. Juillerat-Jeannerat and P. J. Dyson, *Inorg. Chem.*, 2006, **45**, 9006.
23 C. Scolaro, A. Bergamo, L. Brescacin, R. Delfino, M. Cocchietto, G. Laurenczy, T. J. Geldbach, G. Sava and P. J. Dyson, *J. Med. Chem.*, 2005, **48**, 4161.

24 A. Bergamo, C. Gaiddon, J. H. M. Schellens, J. H. Beijnen and G. Sava, *J. Inorg. Biochem.*, 2012, **106**, 90.
25 P. Nowak-Sliwinska, J. R. van Beijnum, A. Casini, A. A. Nazarov, G. Wagnieres, H. van den Bergh, P. J. Dyson and A. W. Griffioen, *J. Med. Chem.*, 2011, **54**, 3895.
26 A. Weiss, B. H. Berndsen, M. Dubois, M. Müller, R. Schibli, A. W. Griffioen, P. J. Dyson and P. Nowak-Sliwinska, *Chem. Sci.*, 2014, **5**, 4742.
27 P. Bergamini, L. Marvelli, A. Marchi, F. Vassanelli, M. Fogagnolo, P. Formaglio, T. Bernardi, R. Gavioli and F. Sforza, *Inorg. Chim. Acta*, 2012, **391**, 162.
28 A. K. Renfrew, L. Juillerat-Jeanneret and P. J. Dyson, *J. Organomet. Chem.*, 2011, **696**, 772.
29 F. A. Khan, B. Therrien, G. Suss-Fink, O. Zava and P. J. Dyson, *J. Organomet. Chem.*, 2013, **730**, 49.
30 G. Suss-Fink, F. A. Khan, L. Juillerat-Jeanneret, P. J. Dyson and A. K. Renfrew, *J. Cluster Sci.*, 2010, **21**, 313.
31 M. Fandzloch, A. Jaromin, M. Zaremba-Czogalla, A. Wojtczak, A. Lewińska, J. Sitkowski, J. Wiśniewska, I. Łakomska and J. Gubernator, *Dalton Trans.*, 2020, **49**, 1207.
32 I. Łakomska, M. Fandzloch, T. Muzioł, T. Lis and J. Jezierska, *Dalton Trans.*, 2013, **42**, 6219.
33 I. Łakomska and M. Fandzloch, *Coord. Chem. Rev.*, 2016, **327–328**, 221.
34 A. B. Caballero, A. Rodriguez-Diéguez, M. Quirós, J. M. Salas, Ó. Huertas, I. Ramirez-Macias, F. Olmo, C. Martin, G. Chaves-Lemaur, R. Gutierrez-Sánchez and M. Sánchez-Moreno, *Eur. J. Med. Chem.*, 2014, **85**, 526.
35 A. B. Caballero, A. Rodríguez-Diéguez, J. M. Salas, M. Sánchez-Moreno, C. Marín, I. Ramírez-Macías, N. Santamaría-Díaz and R. Gutiérrez-Sánchez, *J. Inorg. Biochem.*, 2014, **138**, 39.
36 J. M. Méndez-Arriaga, A. Rodríguez-Diéguez and M. Sánchez-Moreno, *Polyhedron*, 2020, **176**, 114272.
37 J. M. Méndez-Arriaga, I. Oyarzabal, G. Escolano, A. Rodríguez-Diéguez, M. Sánchez-Moreno and J. M. Salas, *J. Inorg. Biochem.*, 2018, **180**, 26.
38 G. M. Esteban-Parra, J. M. Méndez-Arriaga, A. Rodríguez-Diéguez, M. Quirós, J. M. Salasa and M. Sánchez-Moreno, *J. Inorg. Biochem.*, 2019, **201**, 110810.
39 K. Stuart, R. Brun, S. Croft, A. Fairlamb, R. E. Gürtler, J. McKerrow, S. Reed and R. Tarleton, *J. Clin. Invest.*, 2008, **118**, 1301.
40 A. B. Caballero, J. M. Salas and M. Sánchez-Moreno, in *Metal Based Therapeutics for Leishmaniasis. Leishmaniasis-Trends in Epidemiology, Diagnosis and Treatment*, ed. D. M. Claborn, InTech Publishing, Rijeka, Croatia, 2014, ISBN: 978-953-51-1232-7.
41 S. L. Croft, M. P. Barrett and J. A. Urbina, *Trends Parasitol.*, 2005, **21**(11), 508.
42 A. Martínez, T. Carreon, E. Iniguez, A. Anzellotti, A. Sánchez, M. Tyan, A. Sattler, L. Herrera, R. A. Maldonado and R. A. Sánchez-Delgado, *J. Med. Chem.*, 2012, **55**, 3867.
43 https://www.liverpool.ac.uk/pfg/Research/Tools/BuffferCalc/Buffer.html.
44 J. M. Balkaran, S. C. P. van Bezouw, J. van Bruchem, J. Verasdonck, P. C. Verkerk, A. G. Volbeda, I. Mutikainen, U. Turpeinen, G. A. van Albada and P. Gamez, *Inorg. Chim. Acta*, 2009, **362**, 861.
45 J. H. Adriaanse, S. H. C. Askes, Y. van Bree, S. van Oudheusden, E. D. van den Bos, E. Günay, I. Mutikainen, U. Turpeinen, G. A. van Albada, J. G. Haasnoot and J. Reedijk, *Polyhedron*, 2009, **28**, 3143.
46 C. Bülow and K. Haas, *Ber. Dtsch. Chem. Ges.*, 1909, **42**, 4638.
47 S. Jensen, S. Rodger and M. Spicer, *J. Organomet. Chem.*, 1998, **556**, 151.
48 G. Mestroni, E. Alessio and G. Sava, New salts of anionic complexes of Ru(III) as antimetastatic and antineoplastic agents, *International Patent WO*, 98/00431, 1998.
49 J. Furrer, *Chem. Commun.*, 2010, **46**, 3396.
50 E. Kupce and R. Freeman, *Magn. Reson. Chem.*, 2007, **45**, 2.
51 *Rigaku Oxford Diffraction. CrysAlisPro Software System, version 1.171.38.41*, Rigaku Corporation, Oxford, UK, 2015.
52 G. M. Sheldrick, *Acta Crystallogr., Sect. A: Found. Crystallogr.*, 2008, **64**, 112.
53 G. M. Sheldrick, *Acta Crystallogr., Sect. C: Struct. Chem.*, 2015, **71**, 3.
54 C. F. Macrae, I. J. Bruno, J. A. Chisholm, P. R. Edgington, P. McCabe, E. Pidcock, L. Rodriguez-Monge, R. Taylor, J. Van De Streek and P. A. Wood, *J. Appl. Crystallogr.*, 2008, **41**, 466.
55 http://www.povray.org/.
56 A. Albert, *Selective Toxicity. The Physico-Chemical Basis of Therapy*, Chapman and Hall, London, 1979, pp. 662–664.
57 P. González, C. Marín, I. Rodríguez-González, A. B. Hitos, M. J. Rosales, M. Reina, J. G. Díaz, A. Gonzáles-Coloma and M. Sánchez-Moreno, *Int. J. Antimicrob. Agents*, 2005, **25**, 136.
58 O. Trott and A. J. Olson, *J. Comput. Chem.*, 2010, **31**, 455.
59 G. Jones, P. Willett, R. C. Glen, A. R. Leach and R. Taylor, *J. Mol. Biol.*, 1997, **267**, 727.
60 M. J. Frisch, G. W. Trucks, H. B. Schlegel, *et al.*, *Gaussian, Version 16*, Gaussian, Inc., Wallingford, CT, USA, 2016.
61 J. D. Chai and M. Head-Gordon, *J. Chem. Phys.*, 2008, **128**, 084106.
62 J. D. Chai and M. Head-Gordon, *Phys. Chem. Chem. Phys.*, 2008, **10**, 6615.
63 F. Weigend and R. Ahlrichs, *Phys. Chem. Chem. Phys.*, 2005, **7**, 3297.
64 D. E. Volk, J. S. Rice, B. A. Luxon, H. J. Yeh, C. Liang, G. Xie, J. M. Sayer, D. M. Jerina and D. G. Gorenstein, *Biochemistry*, 2000, **39**, 14040.
65 A. Bujacz, *Acta Crystallogr., Sect. D: Biol. Crystallogr.*, 2012, **68**, 1278.
66 H. M. Berman, J. Westbrook, Z. Feng, G. Gilliland, T. N. Bhat, H. Weissig, I. N. Shindyalov and P. E. Bourne, *The Protein Data Bank Nucleic Acids Research*, 2000, vol. 28, p. 235.
67 K. V. Miroshnychenko and A. V. Shestopalova, Molecular Docking of Biologically Active Substances to Double Helical

Nucleic Acids: Problems and Solutions, Chapter 5, in *Applied Case Studies and Solutions in Molecular Docking-Based Drug Design (Advances in Medical Technologies and Clinical Practice)*, ed. S. Dastmalchi, M. Hamzeh-Mivehroud and B. Sokouti, IGI Global, USA, Hershey PA, 2016.

68 A. V. Marenich, C. J. Cramer and D. G. Truhlar, *J. Phys. Chem. B*, 2009, **113**, 6378.

69 E. F. Pettersen, T. D. Goddard, C. C. Huang, G. S. Couch, D. M. Greenblatt, E. C. Meng and T. E. Ferrin, UCSF Chimera - a visualization system for exploratory research and analysis, *J. Comput. Chem.*, 2004, **25**(13), 1605.

70 C. F. Macrae, I. Sovago, S. J. Cottrell, P. T. A. Galek, P. McCabe, E. Pidcock, M. Platings, G. P. Shields, J. S. Stevens, M. Towler and P. A. Wood, Mercury 4.0: from visualization to analysis, design and prediction, *J. Appl. Crystallogr.*, 2020, **53**, 226.

71 R. Dennington, T. A. Keith and J. M. Millam, *GaussView, Version 6.1*, Semichem Inc., Shawnee Mission, KS, 2016.

72 S. Yousuf and I. V. Muthu Vijayan Enoch, *AAPS PharmSciTech*, 2013, **14**(2), 770.

73 P. Vaupel, F. Kallinowski and P. Okunieff, *Cancer Res.*, 1989, **49**, 6449.

74 R. A. Gatenby and R. J. Gillies, *Nat. Rev. Cancer*, 2004, **4**, 891.

75 P. Vaupel, F. Rallinowski and P. Okunieff, *Cancer Res.*, 1989, **49**, 6449.

76 F. Kallinowski, K. H. Schienger, S. Runkel, M. Kloes, M. Stohrer, P. Okunieff and P. Vaupcl, *Cancer Res.*, 1989, **49**, 3759.

77 L. Helm and A. E. Merbach, *Chem. Rev.*, 2005, **105**, 1923.

78 M. Fandzloch, J. M. Méndez-Arriaga, M. Sánchez-Moreno, A. Wojtczak, J. Jezierska, J. Sitkowski, J. Wiśniewska, J. M. Salas and I. Łakomska, *J. Inorg. Biochem.*, 2017, **176**, 144.

79 M. Stebler-Röthlisberger, W. Hummel, P. A. Pittet, H. B. Bürgi, A. Ludi and A. E. Merbach, *Inorg. Chem.*, 1988, **27**, 1358.

80 L. Dadci, H. Elias, U. Frey, A. Hornig, U. Koelle, A. E. Merbach, H. Paulus and J. S. Schneider, *Inorg. Chem.*, 1995, **34**, 306.

81 C. Riccardi, D. Musumeci, A. Capuozzo, C. Irace, S. King, I. Russo Krauss, L. Paduano and D. Montesarchio, *ACS Biomater. Sci. Eng.*, 2018, **4**(1), 163.

82 E. Namiecińska, B. Sadowska, M. Więckowska-Szakiel, A. Dołęga, B. Pasternak, M. Grazul and E. Budzisz, *RSC Adv.*, 2019, **9**, 38629.

83 I. Łakomska, K. Stefańczak, M. Fandzloch, J. Sitkowski, B. Filip-Psurska and A. Wojtczak, *Polyhedron*, 2016, **109**, 33.

84 R. Panchagnula and N. S. Thomas, *Int. J. Pharm.*, 2000, **201**, 131.

85 X. Li and M. A. Cooper, *Anal. Chem.*, 2012, **84**, 2609.

86 M. Pagano, B. Demoro, J. Toloza, L. Boiani, M. González, H. Cerecetto, C. Olea-Azar, E. Norambuena, D. Gambino and L. Otero, *Eur. J. Med. Chem.*, 2009, **44**, 4937.

87 R. Kumar Gupta, G. Sharma, R. Pandey, A. Kumar, B. Koch, P.-Z. Li, Q. Xu and D. Shankar Pandey, *Inorg. Chem.*, 2013, **52**, 13984.

88 R. Vijayalakshmi, M. Kanthimathi, R. Parthsarathi and B. U. Nair, *Bioorg. Med. Chem.*, 2006, **14**, 3300.

89 L. Messori, P. Orioli, D. Vullo, E. Alessio and E. Iengo, *Eur. J. Biochem.*, 2000, **267**, 1206.

90 H. Sun, H. Li and P. J. Sadler, *Chem. Rev.*, 1999, **99**, 2817.

91 S. P. Young, A. Bomford and R. Williams, *Biochem. J.*, 1984, **219**, 505.

92 P. Lincoln, E. Tuite and B. Norden, *J. Am. Chem. Soc.*, 1997, **119**, 1454.

93 A. Martínez, J. Suárez, T. Shand, R. S. Magliozzo and R. A. Sánchez-Delgado, *J. Inorg. Biochem.*, 2011, **105**, 39.

94 L. Messori, P. Orioli, D. Vullo, E. Alessio and E. Iengo, *Eur. J. Biochem.*, 2000, **267**, 1206.

95 M. Fandzloch, L. Dobrzańska, T. Jędrzejewski, J. Jezierska, J. Wiśniewska and I. Łakomska, *J. Biol. Inorg. Chem.*, 2020, **25**, 109.

96 M. Fandzloch, L. Dobrzańska, J. Jezierska, B. Filip-Psurska, J. Wiśniewska, J. Wietrzyk, J. M. Salas and I. Łakomska, *Polyhedron*, 2018, **141**, 239.

97 M. Fandzloch, A. Wojtczak, J. Wiśniewska, K. Stefańczak, J. M. Salas and I. Łakomska, *Inorg. Chim. Acta*, 2016, **443**, 170.

98 Unpublished results.